

RePoseD: Efficient Relative Pose Estimation With Known Depth Information

Yaqing Ding¹, Viktor Kocur², Václav Vávra¹, Jian Yang³, Torsten Sattler⁴, and Zuzana Kukelova¹

¹ Visual Recognition Group, Faculty of Electrical Engineering, Czech Technical University in Prague

² Faculty of Mathematics, Physics and Informatics, Comenius University in Bratislava

³ VCIP, CS, Nankai University, Tianjin, China

⁴ Czech Institute of Informatics, Robotics and Cybernetics, Czech Technical University in Prague

Abstract

Recent advances in monocular depth estimation methods (MDE) and their improved accuracy open new possibilities for their applications. In this paper, we investigate how monocular depth estimates can be used for relative pose estimation. In particular, we are interested in answering the question whether using MDEs improves results over traditional point-based methods. We propose a novel framework for estimating the relative pose of two cameras from point correspondences with associated monocular depths. Since depth predictions are typically defined up to an unknown scale or even both unknown scale and shift parameters, our solvers jointly estimate the scale or both the scale and shift parameters along with the relative pose. We derive efficient solvers considering different types of depths for three camera configurations: (1) two calibrated cameras, (2) two cameras with an unknown shared focal length, and (3) two cameras with unknown different focal lengths. Our new solvers outperform state-of-the-art depth-aware solvers in terms of speed and accuracy. In extensive real experiments on multiple datasets and with various MDEs, we discuss which depth-aware solvers are preferable in which situation. The code will be made publicly available.

1. Introduction

Relative pose estimation is a core problem in a wide range of computer vision applications, including Structure-from-Motion (SfM) [55], visual localization [53, 59, 69], and autonomous robots [41]. Typically, the relative pose of cameras is estimated from 2D-2D image point correspondences that are established using feature matching. Given 2D-2D matches, the relative pose [26, 35, 36, 49, 57, 58] of two cameras can be estimated using the epipolar geometry constraints [27]. For two calibrated cameras, 5 point correspondences are needed to estimate the 5 degrees of freedom of the relative pose (3 for rotation and two for the translation up to an unknown scale) [26, 35, 49, 58]. The relative

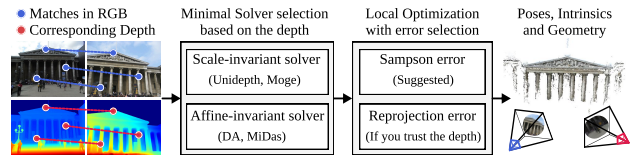


Figure 1. Given point matches and their corresponding depths from a pair of images, we propose the use of different minimal solvers for relative pose estimation, according to the properties of the depth data. For local optimization, the Sampson error is generally more robust across varying depth conditions, while the reprojection error may yield better results when the depth measurements are highly reliable.

pose of two cameras with unknown shared focal length can be estimated from 6 correspondences [26, 35, 36, 57]. If the full intrinsic calibration is unknown and/or both cameras have different calibrations, the relative pose can be estimated from 7 or 8 correspondences [27].

Due to noise in the measurements and the presence of outlier correspondences, algorithms for relative pose estimation are usually employed in RANSAC-style hypothesize-and-verify frameworks [20]. The number of RANSAC iterations grows exponentially with the number of correspondences needed to estimate the pose. As such, a considerable amount of work focuses on reducing the number of correspondences necessary for pose estimation. This is typically done by using additional information, such as the gravity direction from an Inertial Measurement Unit (IMU) [21, 34, 48, 60], or information about the local feature geometry such as the scale and rotation of features [2, 25, 44] or local affine frames [5, 6, 19].

Recently, learning-based methods [9, 23, 28, 46, 51, 62, 65, 66] have achieved significant success in predicting depth from a single image. The increasing precision of Monocular Depth Estimation methods (MDE) opens new possibilities of using depth information in downstream tasks. Recent studies have shown a growing focus on the use of dense depth estimates to improve the performance of various geometry-based applications, including structure-from-

motion/SLAM [43, 47, 70], dense reconstruction [64, 68], and novel view synthesis [29, 40].

Depth naturally provides additional information for camera pose estimation. Thus, several recent works [1, 4] attempted to use monocular depths from MDE networks or networks to estimate the relative depths of two features [17] to improve the relative pose estimation of cameras. The depth information provides additional constraints on the geometry, and thus reduces the number of correspondences necessary for the estimation. However, it also introduces new challenges: (1) Learning-based depth estimates are usually much more noisy and erroneous than image measurements. (2) MDE methods typically produce scale/affine-invariant depth [9, 32, 46, 62], affine-invariant inverse depth [8, 52, 65, 66] or metric depth [7, 28, 51], meaning that the estimated depth or inverse depth is only defined up to an unknown scale factor or both unknown scale and shift parameters. (3) The unknown shift and scale can be different for different images of the same scene. The scale may not even be consistent across an image, *i.e.*, some parts of the image may be scaled by a different scale than others. Due to these challenges and the fact that the solvers proposed in [1, 17] use only relative depths, do not model unknown shifts, and have been tested only with depths from one network (Depth Anything [66] in [17], and a network for estimating the relative depth proposed directly in [1]), [1, 17] do not convincingly show the improvement of their depth-aware solvers over traditional 2D-2D point-based relative pose solvers [27, 49, 58]. Thus, prior work does not answer the question of whether recent MDE networks provide useful information for the relative pose estimation task.

This paper attempts to provide an answer to this question by presenting a comprehensive comparison of different depth-aware solvers for calibrated, shared focal length and different focal lengths cases, under different conditions, *i.e.*, different sources of depth information, different feature detectors and matchers, different types of datasets (interior/exterior) and different optimization schemes inside RANSAC. To this end, we provide novel solvers for three different types of monocular depths: metric depth, scale-invariant depth, and affine-invariant depth. We introduce novel formulations that jointly estimate the relative pose of two cameras along with the scale or affine parameters of the monocular depths. The proposed solvers use the full information from the depth estimates, resulting in fewer correspondences necessary for the relative pose estimation compared to solvers based on relative depths [17].

The main contributions of the paper are:

- We integrate scale and affine parameters of monocular depth into solvers for relative pose estimation. These parameters are estimated together with the relative pose.
- We discuss all possible combinations of known and unknown shift and scale parameters. We propose several

practical and efficient minimal solvers for calibrated cameras, two cameras with shared unknown focal length, and two cameras with different unknown focal lengths. Our solvers outperform state-of-the-art depth-aware solvers in terms of efficiency and accuracy.

- We evaluate different RANSAC schemes to account for potentially erroneous and noisy depth estimates.
- In extensive real experiments, we answer the questions which state-of-the-art MDE networks are suitable for relative pose estimation, which require modeling unknown scale or affine parameters, and which provide the best improvement in terms of efficiency and accuracy over traditional, purely point correspondence-based solvers.

2. Related Work

[44] shown that the relative scales of SIFT [45] features can approximate the inverse relative depths of the features. In this case, one point correspondence provides two constraints for relative pose estimation, and the 5-DOF problem can be solved using only three point correspondences with two relative depths. In the same setting, Guan *et al.* [25] solve the generalized relative pose problem using three SIFT correspondences. Astermark *et al.* [1] propose a closed-form minimal solution to the relative pose of two calibrated pinhole cameras with known relative depth. In addition, they propose a neural network to estimate the relative depth. In [16], relative depths approximated from SIFT scales are used to estimate the calibrated homography. Barath *et al.* [4] propose a 2-point solver with depth information for relative pose estimation. However, as pointed out in [67], this 2-point solver is degenerate for rigid alignments due to rank deficiency. In [17], the authors propose new minimal solvers that use relative depth for fundamental matrix estimation. They discuss different variants of solvers with known and unknown focal lengths. Their solvers work for monocular depths with unknown different scales. However, the solvers do not model unknown shifts in the depths, assuming that the shifts are zero in both images and thus can be ignored. All of the methods and minimal solvers discussed above use only the information from relative depths. Thus, they do not utilize the full information that two monocular depth maps can provide.

Dust3r [63] is a recent 3D foundation model for two-view geometry estimation tasks, including depth prediction and relative pose estimation. The relative pose is estimated by aligning two point maps with a similarity transformation. Trained on large-scale datasets, Dust3r is able to handle scenarios where there is little overlap between the two images. Mast3r [39] further improves performance through feature matching. Mast3r minimizes both 3D-3D matching errors and 3D-2D reprojection errors to refine depths, relative poses, and intrinsic parameters.

In this paper, in contrast to the minimal solvers men-

tioned above that use only relative depths, we solve the problem using the full information from two depth maps. This allows us to formulate the relative pose problem using different combinations of 3D-3D/3D-2D/2D-2D correspondences. One 3D-3D correspondence provides three constraints and allows us to solve the relative pose problem from fewer correspondences than [17]. Moreover, we propose new minimal solvers that model not only unknown scales, but also unknown shifts in depth maps.

Concurrently to our work, Yu *et al.* [67] developed three novel minimal relative pose solvers for affine-invariant depths. Their calibrated, shared-focal, and two-focal length solvers solve the same formulation as our solvers with unknown shift and scales. In order to deal with potentially noisy and erroneous depth information, Yu *et al.* propose to use their depth-aware solvers jointly with classical 2D-2D point-based solvers in a hybrid LO-MSAC [10, 61] framework. In their Madpose framework, they combine the symmetric depth-induced reprojection error and the Sampson error for scoring pose hypotheses and for local optimization. The main differences between our work and [67] are the following: (1) Our solutions to configurations with unknown shifts and scales, *i.e.*, affine-invariant depths, result in smaller and thus faster solvers. For a detailed comparison of sizes and run-times of the proposed and the Madpose solvers [67], see Table 2. (2) In addition to affine-invariant solvers, we also derive novel minimal solvers for cases with known/zero shifts and either unknown or known/same scales. Moreover, we derive a calibrated solver for inverse depth and discuss the number of solutions for all other variants of known/unknown/same/different shifts and scales (see Table 1). (3) By testing more variants of solvers, including novel solvers with zero shifts, we show that in some scenarios it is not necessary to model unknown shifts. This is in contrast to the observation made by [67], who, by missing some variants of the solvers in their experiments, concluded that modeling the unknown shift is always beneficial (even for “metric” depths). (4) In contrast to using a complex hybrid RANSAC scheme and a combination of reprojection and Sampson errors that results in slower running times, we look at a simple and more efficient local optimization scheme based on using a single solver with either reprojection or Sampson error. Even for 3D points, we propose to compose the essential/fundamental matrix and measure the Sampson error, as this usually leads to better results.

3. Problem Statement

Assume that a set of 3D points Ω is observed by two cameras with projection matrices $\mathbf{K}_1[\mathbf{I} \mid \mathbf{0}]$ and $\mathbf{K}_2[\mathbf{R} \mid \mathbf{T}]$. Let $\{\mathbf{p}_i, \mathbf{q}_i\}, i = 1, \dots, n$ be a set of n 2D point correspondences, *i.e.*, the projections of 3D points Ω in the first and

the second camera, respectively. Then we have

$$\lambda_i \mathbf{K}_2^{-1} \mathbf{q}_i = \eta_i \mathbf{R} \mathbf{K}_1^{-1} \mathbf{p}_i + \mathbf{T}, \quad (1)$$

where λ_i and η_i are the depths of the points \mathbf{q}_i and \mathbf{p}_i .

MDE networks provide either scale/affine-invariant depth [9, 32, 46, 62], affine-invariant inverse depth [8, 52, 65, 66], or metric depth [7, 28, 51]. In most general case of affine-invariant depth the true depths λ_i and η_i in (1) can be expressed as

$$\eta_i = s_1(\alpha_i + u), \quad \lambda_i = s_2(\beta_i + v), \quad (2)$$

where α_i, β_i are estimated affine-invariant depths, and $\{s_1, s_2\}, \{u, v\}$ are the unknown scales and shifts of the depths. Substituting (2) into (1), we have

$$s_2(\beta_i + v) \mathbf{K}_2^{-1} \mathbf{q}_i = s_1(\alpha_i + u) \mathbf{R} \mathbf{K}_1^{-1} \mathbf{p}_i + \mathbf{T}, \quad (3)$$

Dividing (3) by s_1 , results in

$$s(\beta_i + v) \mathbf{K}_2^{-1} \mathbf{q}_i = (\alpha_i + u) \mathbf{R} \mathbf{K}_1^{-1} \mathbf{p}_i + \mathbf{t}, \quad (4)$$

where $s = s_2/s_1$ and $\mathbf{t} = \mathbf{T}/s_1$, *i.e.* two different scales are replaced by the relative scale s . Note that in this case, the scale of the translation \mathbf{t} is defined w.r.t. s_1 , thus we can not further fix the scale of \mathbf{t} , *i.e.* the translation vector is not estimated up to scale like in the standard relative pose solvers [49], but needs to be estimated as a 3 degrees of freedom (3-DOF) vector. This means that for calibrated cameras, *i.e.*, for known calibration matrices \mathbf{K}_1 and \mathbf{K}_2 , we have a 9-DOF problem w.r.t. $\{s, u, v, \mathbf{R}, \mathbf{t}\}$. Since one 3D-3D point correspondence¹ provides three constraints of the form (4), we need at least 3 point correspondences with their monocular depths to solve this problem for the calibrated case. For the case of unknown focal lengths f_1 and f_2 in calibration matrices \mathbf{K}_1 and \mathbf{K}_2 , we have 10 and 11 DoF, for cases $f_1 = f_2$ and $f_1 \neq f_2$ respectively.

In addition to affine-invariant depths, some MDE networks provide scale-invariant depths or even metric depths; moreover, in some applications the depth can be estimated directly using depth sensors. Thus in some scenarios, we can assume known/zero shift and/or equal scales and shifts of two depths. There are 6 possible combinations of known and unknown shifts and scales that result in different DOF problems. Table 1 lists all these combinations together with the number of solutions for different problem settings, with novel solvers to interesting practical setups that are tested in the main paper and in the Supplemental Material (SM) highlighted in red and blue, respectively. Note that for calibrated case the setups with known shifts and scales ($\{s, u, v\} = \{1, 0, 0\}$), and with known shifts and unknown

¹Note that in this case the 2D points $\{\mathbf{p}_i, \mathbf{q}_i\}$ are equipped with depths and thus lifted to 3D points.

	Solver	Point Correspondence			Scale Ratio	Shift	DOF	No. of Solutions
		3D-3D	3D-2D	2D-2D				
Calibrated	5-point [49]	-	-	5	-	-	5	10
	Rel3PT* [11]	2	-	1	1	(0, 0)	5	4
	P3P [15]	-	3	-	s	(0, -)	6	4
	3PT _{1uv}	1	2	0	1	(u, u)	7	8
	3PT _{1uv}	2	1	0	1	(u, v)	8	8
	3PT _{suv}	2	1	0	s	(u, u)	8	8
	3PT _{suv}	3	0	0	s	(u, v)	9	4
	3PT _{suv} (inverse)	3	0	0	s	(u, v)	9	10
	6-point [26]	-	-	6	-	-	6	15
	3p3d* [17]	3	-	-	1	(0, 0)	6	4
Equal f	3PT _{100f}	1	2	0	1	(0, 0)	7	6
	3PT _{1uvf}	2	1	0	1	(u, u)	8	6
	3PT _{1uvf}	3	0	0	1	(u, v)	9	4
	3PT _{s00f}	2	1	0	s	(0, 0)	8	4
	3PT _{suvf}	3	0	0	s	(u, u)	9	6
	4PT _{suvf}	3	0	1	s	(u, v)	10	8
	7-point [27]	-	-	7	-	-	7	3
	4p4d* [17]	4	-	-	s	(0, 0)	7	1
Varying f_1, f_2	3PT _{100f_{1,2}}	2	1	0	1	(0, 0)	8	3
	3PT _{1uvf_{1,2}}	3	0	0	1	(u, u)	9	4
	4PT _{1uvf_{1,2}}	3	0	1	1	(u, v)	10	16
	3PT _{s00f_{1,2}}	3	0	0	s	(0, 0)	9	1
	4PT _{suvf_{1,2}}	3	0	1	s	(u, u)	10	18
	4PT _{suvf_{1,2}}	3	1	0	s	(u, v)	11	4

Table 1. Different combinations of using 3D-3D, 3D-2D and 2D-2D point correspondences for focal length problems. The blue and red markers represent the solvers used in our experiments. Note that subscripts suv in names of the solvers represent different configurations of known/unknown/same/different scales and shifts in the depth maps. *Relative depth was used, where one partial 3D-3D correspondence provides only 2 constraints.

scale $\{s, u, v\} = \{s, 0, 0\}$ can be solved using the well-known P3P solver [15, 22, 50]. The P3P solver can handle scale invariant depth, since it only uses single side depth.² Due to space limits, we only discuss two practical scenarios in the main paper: the two depths up to unknown scale with two different shifts, and the two depth maps up to unknown scale. Other cases are discussed in the SM.

3.1. Calibrated Case

In this section, we first discuss the solver for calibrated case, where the intrinsic parameters of cameras are known, *i.e.*, \mathbf{K}_1 and \mathbf{K}_2 are known. We use $\tilde{\mathbf{q}}_i = \mathbf{K}_2^{-1}\mathbf{q}_i$, $\tilde{\mathbf{p}}_i = \mathbf{K}_1^{-1}\mathbf{p}_i$ to represent the normalized image points.

Given 3 point correspondences and their monocular depths, substituting $\tilde{\mathbf{q}}_i, \tilde{\mathbf{p}}_i$, $i = 1, 2, 3$ into (4) we have nine equations in nine unknowns

$$s(\beta_i + v)\tilde{\mathbf{q}}_i = (\alpha_i + u)\mathbf{R}\tilde{\mathbf{p}}_i + \mathbf{t}. \quad (5)$$

By eliminating the translation from the above equations, *i.e.*, by subtracting pairs of equations, we have

$$s(\beta_i + v)\tilde{\mathbf{q}}_i - s(\beta_j + v)\tilde{\mathbf{q}}_j = \mathbf{R}((\alpha_i + u)\tilde{\mathbf{p}}_i - (\alpha_j + u)\tilde{\mathbf{p}}_j),$$

for $(i, j) = (1, 2), (1, 3), (2, 3)$.

²Although one 3D-3D point correspondence provides three constraints, we can not use only two 3D-3D point correspondences to solve 6-DOF pose problem with known $\{s, u, v\} = \{1, 0, 0\}$. The reason is that the rotation cannot be determined with only two points. There still remains a 1-DOF rotation around the line passing through the two points.

Solver	G-J	Eigen	Time (μ s)
3PT _{suv} (Ours)	3×6	Closed-form	1.46
3PT _{suv} (M)	12×16	4×4	4.45
4PT _{suvf} (Ours)	24×32	8×8	12.5
4PT _{suvf} (M)	36×44	8×8	23.6
4PT _{suvf_{1,2}} (Ours)	20×24	4×4	6.45
4PT _{suvf_{1,2}} (M)	40×44	4×4	20.2

Table 2. Efficiency Comparison between the proposed affine-invariant solvers and those from Madpose [67], denoted as (M).

Since applying the rotation matrix on a vector preserves the length of this vector, we have the following constraints

$$\|s(\beta_i + v)\tilde{\mathbf{q}}_i - s(\beta_j + v)\tilde{\mathbf{q}}_j\| = \|(\alpha_i + u)\tilde{\mathbf{p}}_i - (\alpha_j + u)\tilde{\mathbf{p}}_j\|,$$

for $(i, j) = (1, 2), (1, 3), (2, 3)$. In this case, the rotation is eliminated and we obtain three equations in three unknowns. Since the equations only contain s^2 , we can let $c = s^2$ to reduce the degrees and eliminate the symmetries. In short, if s is a solution, then $-s$ is also a solution. However, s should be positive since it presents the relative scale of two depths. thus a solution to $c = s^2$ gives us only one geometrically feasible solution for s .

The three above equations can be written in a matrix form $\mathbf{M} [cv^2, cv, c, u^2, u, 1]^T = 0$, where \mathbf{M} is a 3×6 coefficient matrix. After Gauss-Jordan (G-J) elimination of this matrix, the three monomials $\{cv^2, cv, c\}$ can be expressed as quadratic functions of u , *i.e.*, $cv^2 = g_1(u)$, $cv = g_2(u)$, $c = g_3(u)$, where g_1, g_2, g_3 are polynomials in u of degree 2. Since $(cv)^2 = (c)(cv^2)$, we have $g_2^2 = g_1g_3$, resulting in a quartic equation in u . This equation can be solved in closed form. We denote the final solver as 3PT_{suv}. Note that the inverse depth model results in a more complex solver without improving performance in our experiments (details provided in the SM). Therefore, we do not discuss the inverse depth model in the main paper.

3.2. Focal Length Problems

In many practical scenarios, the intrinsic parameters of the cameras may not be available. However, it is often reasonable to assume that modern cameras have square-shaped pixels, and the principal point coincides with the image center [26]. This is a widely used assumption in many camera geometry solvers, where the only unknown intrinsic parameters are focal lengths, *i.e.*, $\mathbf{K}_i = \text{diag}(f_i, f_i, 1)$.

Shared Unknown Focal Length

First, let us assume that the two cameras have a shared unknown focal length, *i.e.*, $\mathbf{K}_1 = \mathbf{K}_2 = \text{diag}(f, f, 1)$, which is a common scenario, *e.g.*, when estimating the motion of a single uncalibrated camera. This is a 10-DOF problem w.r.t. $\{s, u, v, \mathbf{R}, \mathbf{t}, f\}$, and we need at least three 3D-3D point correspondences and one 2D-2D point correspondence, *i.e.* four 2D-2D correspondences from which three have monocular depths estimated in both images and thus can be considered as 3D-3D correspondences. Note that,

here the 3D-3D point correspondences depend on the unknown focal length parameter.

In this case, we may obtain the following system of 6 equations in 6 unknowns $\{s, u, v, f, \eta_4, \lambda_4\}$

$$\begin{aligned} \|s\mathbf{K}_2^{-1}((\beta_i + v)\mathbf{q}_i - s(\beta_j + v)\mathbf{q}_j)\| &= \|\mathbf{K}_1^{-1}((\alpha_i + u)\mathbf{p}_i - (\alpha_j + u)\mathbf{p}_j)\|, \\ \|s\mathbf{K}_2^{-1}((\beta_k + v)\mathbf{q}_k - \lambda_4\mathbf{q}_4)\| &= \|\mathbf{K}_1^{-1}((\alpha_k + u)\mathbf{p}_k - \eta_4\mathbf{p}_4)\|, \end{aligned}$$

for $(i, j) = (1, 2), (1, 3), (2, 3)$ and $k = 1, 2, 3$. To solve such a system, we need to perform G-J elimination of a large matrix. Moreover, the system has up to 28 real solutions. Thus, its solver is not practically relevant.

To find a more efficient and practical solution, we use four 2D-2D point correspondences with their four depths in both images. In this case, we obtain the following 6 equations in 4 unknowns $\{s, u, v, f\}$

$$\|s\mathbf{K}_2^{-1}((\beta_i + v)\mathbf{q}_i - (\beta_j + v)\mathbf{q}_j)\| = \|\mathbf{K}_1^{-1}((\alpha_i + u)\mathbf{p}_i - (\alpha_j + u)\mathbf{p}_j)\|,$$

where $i, j = 1, 2, 3, 4$, $i \neq j$. In general, it is an over-constrained system. One way to solve it is to use four of these six equations in four unknowns. The system of four polynomials can be solved using the Gröbner basis method [38], where the final solver performs G-J elimination of a 24×32 matrix and extracts up to 8 real solutions from the eigenvalues and eigenvectors of an 8×8 matrix. We denote this solver as $\mathbf{4PT}_{suvf}$. Alternatively, by using all six equations, we can derive a significantly smaller solver with up to two real solutions. This solver only needs to perform the G-J elimination of a 6×8 matrix. However, it is more sensitive to noise. Further details on this simplified focal length solver are provided in the SM.

With scale invariant depth, we have an 8-DOF problem w.r.t. $\{s, \mathbf{R}, \mathbf{t}, f\}$. We need at least two 3D-3D point correspondences and one 3D-2D point correspondence. The problem can be solved similarly as the calibrated case shown in Sec. 3.1. Due to the space limits, the details are shown in the SM, where we show a general solution to all problem configurations using three point correspondences.

Different and Unknown Focal Lengths

Finally, we consider the case where $\mathbf{K}_i = \text{diag}(f_i, f_i, 1)$, $i = 1, 2$, with $f_1 \neq f_2$. This is a 11-DOF problem w.r.t. $\{s, u, v, \mathbf{R}, \mathbf{t}, f_1, f_2\}$. Thus, we need at least three 3D-3D point correspondences and one 3D-2D point correspondence, *i.e.* a correspondence where we have monocular depth only in one image. Similarly to the equal and unknown focal length case, we can formulate this problem using a system of 6 equations in 6 unknowns with up to 14 real solutions and solved it using [38].

However, a more efficient solver can be obtained using four 3D-3D point correspondences, which yields six equations in five unknowns: s, u, v, f_1, f_2 . This is an over-constrained system that can be again solved by using only five of these six equations. The five equations can be

rewritten as $\mathbf{M} [1, c, f_1, u f_1, u^2 f_1, c f_2, c v f_2, c v^2 f_2]^\top = 0$, where \mathbf{M} is a 5×8 . Here, f_2 always appears together with c , thus, we let $c f_2 = \tilde{f}_2$ to simplify the polynomials. In this case, we obtain a solver that performs the G-J elimination of a 20×24 matrix and results in up to four solutions. We denote this solver as $\mathbf{4PT}_{suvf_{1,2}}$. Alternatively, we can use all six equations to derive a smaller solver, which is faster, but more sensitive to noise (see SM for more details).

With scale-invariant depth, we have a 9-DOF problem w.r.t. $\{s, \mathbf{R}, \mathbf{t}, f_1, f_2\}$. We need at least three 3D-3D point correspondences. This problem can be solved similarly as the calibrated case shown in Sec. 3.1. Due to space limits, the details on this $\mathbf{3PT}_{s00f_{1,2}}$ solver are shown in the SM.

4. Experiments

In this section, we present a comprehensive comparison of different depth-aware and point-based solvers for calibrated, shared focal length and different focal length cases, under different conditions, *i.e.* different sources of depth information, different feature detectors and matchers, different type of datasets (interior/exterior) and different optimization schemes inside RANSAC.

Solvers. (1) For the calibrated relative pose estimation, we compare our $\mathbf{3PT}_{suvf}$ (ours) solver with the solver $\mathbf{3PT}_{suvf}(\mathbf{M})$ from [67], the Rel3PT solver [1], the P3P solver [15], and the 5PT point-based solver [49]. (2) For the unknown shared focal length case, we compared the proposed $\mathbf{3PT}_{s00f}$ (ours) and $\mathbf{4PT}_{suvf}$ (ours) solvers with the $\mathbf{4PT}_{suvf}(\mathbf{M})$ solver from [67], the 3p3d solver [17] and the 6PT point-based solver [38]. (3) For the different focal length case, we compare our $\mathbf{3PT}_{s00f_{1,2}}$ (ours) and $\mathbf{4PT}_{suvf_{1,2}}$ (ours) solvers with the $\mathbf{4PT}_{suvf_{1,2}}(\mathbf{M})$ solver from [67], the 4p4d solver [17] and the 7PT solver [27].

Datasets. In order to test the proposed solvers on real-world data, we choose the Phototourism [30], the ETH3D [56] and the ScanNet [13] datasets. The images of the Phototourism dataset were collected from multiple cameras obtained at different times, from different viewpoints, and with occlusions. It is a challenging outdoor dataset that is commonly used as a benchmark dataset [30] for camera geometry methods. We used five test scenes with 24,750 image pairs from this dataset. The ETH3D multi-view stereo and 3D reconstruction benchmark [56] includes a range of indoor and outdoor scenes. Ground truth geometry was acquired using a high-precision laser scanner. Images were captured with a DSLR camera and a synchronized multi-camera rig featuring cameras with varying fields of view. In total, 4,144 image pairs were used from the ETH3D dataset, and we used triangulation to obtain the ground truth depths. The ScanNet dataset is an indoor RGB-D video dataset containing 2.5 million views in more than 1500 scans, annotated with 3D camera poses and surface reconstructions. We followed the evaluation setup in [54], and used 1500

pairs from ScanNet for testing.

Feature Detection and Matching. We used three different image features, the first is the popular sparse SuperPoint (SP) features [14], widely used in SfM and localization pipelines [53]. For SuperPoint matching, we employ LightGlue (LG) [42], a state-of-the-art deep learning-based method that demonstrates significant improvements over traditional matching methods. The second is RoMa [18], a state-of-the-art dense matcher. The last is Mast3r [39], where feature matching is considered as a 3D task with DUS3R [63], a recent and powerful 3D reconstruction framework based on Transformers.

Depth Estimation. We use five state-of-the-art MDE methods to obtain depth data, including MiDas [8], DA v2 (Depth Anything v2) [66], UniDepth [51], MoGe [62], and Mast3r [39]. These MDE methods represent scale/affine-invariant [8, 39, 62, 66] as well as metric depths [51].

Robust Estimation Frameworks. We evaluated all solvers using the LO-RANSAC framework [11] within PoseLib [37] with Sampson error for LO and scoring with an error threshold set at 2 px and fixed 1000 RANSAC iterations. We provide additional experiments using the reprojection error in the SM. We also evaluated selected solvers using the Hybrid RANSAC framework presented in [67] with 2 px Sampson error and 16 px reprojection error thresholds with equal weight for both types of error and fixed 1000 iterations. For Mast3r [39], we use their non-linear optimization with 500 iterations for coarse refinement and 200 iterations for fine refinement. We observe that Mast3r performs better in our evaluation compared to the results reported in [67]. We attribute this potentially to using more refinement iterations, which in our experience improves performance.

Evaluation Metrics. In experiments, we report the median pose error ϵ calculated as the maximum of rotation and translation errors in degrees. We also report the mean average accuracy (mAA) [30] with a threshold of 10 degrees. For the focal length solvers we use $f_{err} = |f_{est} - f_{gt}|/f_{gt}$ as the focal length error for one camera. When two cameras with different focal lengths are considered, we use the geometric mean of their errors. We report the median focal length errors denoted as ϵ_f . We also report the mean average accuracy for focal lengths [33] at the 10% error threshold, denoted as mAA_f . Run-times τ are reported in milliseconds. Run-times for all methods except Mast3r are reported per one CPU of Intel Xeon Gold 6338. The run-times of Mast3r are reported on the CPU of Intel I7-11700KF with RTX 3090 GPU. The run-times of all the methods do not include the feature matching and depth estimation since they are equal for all depth-based solvers. For a fair comparison, for Mast3r, we only measure the run-times of the non-linear optimization, *i.e.* time without feature matching, and initial depth estimation. For datasets with multiple scenes, we re-

port the mean values across the scenes.

4.1. Calibrated Relative Pose Estimation

Table 3 shows the comparison of different methods on the ETH3D dataset. The results for the Phototourism and ScanNet datasets are provided in the SM. The results show that using depth in pose estimation results in more accurate poses when good depth estimates (e.g. MoGe [62], UniDepth [51]) are available. In this case, the overall best-performing methods use the hybrid RANSAC proposed in [67] with our solver 3PT_{su v} (ours) slightly outperforming 3PT_{su v} (M) [67]. We note that the use of the hybrid RANSAC scheme comes at a significant increase in computational cost over the use of PoseLib [37]. As the authors of [67] point out, their implementation of the hybrid RANSAC scheme, which we use in our experiments, could be optimized for computational efficiency. However, even with optimizations the method requires significantly more computation per one iteration than standard RANSAC.

Based on the results for PoseLib [37], when good depth is available, P3P [15] performs better than solvers which also model shift. When less accurate depth estimates are available, the 5PT performs best especially with good matches (e.g., Mast3r [39], RoMA [18]). This opens up potential for future work, which would incorporate the P3P solver into the hybrid RANSAC scheme proposed in [67].

4.2. Shared Unknown Focal Length

Table 4 shows the comparison of the methods on the ETH3D dataset [56] for two cameras with a shared unknown focal length. When a good depth estimate is available, the best results are obtained utilizing the hybrid RANSAC scheme from [67]. We show that our solver 3PT_{s 00} f outperforms 4PT_{su v} f (M) [67] for many combinations of MDEs and matches despite not modeling shift. Our 3PT_{s 00} f solver also performs best when comparing solvers incorporated within PoseLib [37] and used in combination with MoGe [62], UniDepth [51] and Mast3r [39]. For DA v2 [66] and MiDas [8] modeling shift seems to be beneficial, and we show that our 4PT_{su v} f solver performs on par with 4PT_{su v} f (M) while being 2x faster. Our observation that modeling an unknown shift is not always necessary is in contradiction to the observation made in [67]. The reason is that [67], have not tested a scale-invariant 3PT solver and have not incorporated other depth-aware solvers into the hybrid ransac scheme. We also note that despite performing expensive non-linear optimization to obtain the poses Mast3r [39] performs worse than approaches based on RANSAC when either good depth (UniDepth [51], MoGe [62]) or matches (RoMA [18]) are available.

A comparison of speed-accuracy tradeoff of various methods is shown in Figure 2 for the combination of RoMA [18] and UniDepth [51]. The figure shows that when

Depth	Solver	Opt.	SP+LG [14, 42]			RoMA [18]		
			$\epsilon(^{\circ}) \downarrow$	mAA \uparrow	$\tau(ms) \downarrow$	$\epsilon(^{\circ}) \downarrow$	mAA \uparrow	$\tau(ms) \downarrow$
Real Depth	5PT [49]	S	0.91	87.67	48.14	0.56	91.10	184.36
	Rel3PT [1]	S	0.88	88.21	103.18	0.52	91.38	532.02
	P3P [15]	S	0.83	88.88	29.68	0.52	91.33	141.39
	3PT _{su0} (M) [67]	S	0.79	88.55	41.81	0.45	91.39	145.59
	3PT _{su0} (ours)	S	0.80	88.60	29.59	0.47	91.37	127.81
	3PT _{su0} (M) [67]	H [67]	0.52	91.39	549.59	0.39	92.73	1505.19
3PT _{su0} (ours)	H [67]	0.52	91.42	543.48	0.39	92.72	1490.93	
MiDas [8]	Rel3PT [1]	S	4.81	71.25	36.34	3.23	82.22	149.63
	P3P [15]	S	0.94	86.16	22.97	0.60	90.80	91.36
	3PT _{su0} (M) [67]	S	0.88	87.34	31.11	0.58	90.77	79.17
	3PT _{su0} (ours)	S	0.88	87.39	20.40	0.59	90.76	67.13
	3PT _{su0} (M) [67]	H [67]	1.08	85.38	685.32	0.67	90.49	1605.43
	3PT _{su0} (ours)	H [67]	1.07	85.45	683.39	0.67	90.50	1590.71
DA v2 [66]	Rel3PT [1]	S	5.57	68.46	35.74	3.90	80.56	145.85
	P3P [15]	S	0.90	86.25	23.26	0.72	90.61	93.99
	3PT _{su0} (M) [67]	S	0.90	87.19	32.50	0.56	90.99	88.60
	3PT _{su0} (ours)	S	0.91	87.07	21.68	0.56	91.01	75.87
	3PT _{su0} (M) [67]	H [67]	0.97	85.52	605.63	0.54	90.62	1493.75
	3PT _{su0} (ours)	H [67]	0.98	85.56	593.95	0.54	90.62	1477.73
MoGe [62]	Rel3PT [1]	S	4.74	72.08	42.19	2.74	82.04	170.29
	P3P [15]	S	0.91	87.67	25.72	0.54	91.16	111.74
	3PT _{su0} (M) [67]	S	0.89	87.71	33.45	0.53	91.04	98.20
	3PT _{su0} (ours)	S	0.89	87.67	22.41	0.54	91.05	84.24
	3PT _{su0} (M) [67]	H [67]	0.86	88.26	566.16	0.50	91.17	1414.96
	3PT _{su0} (ours)	H [67]	0.85	88.24	554.79	0.49	91.23	1401.61
UniDepth [51]	Rel3PT [1]	S	1.36	78.82	49.70	0.70	88.25	207.86
	P3P [15]	S	0.88	88.00	25.93	0.56	91.11	112.65
	3PT _{su0} (M) [67]	S	0.94	87.42	33.90	0.55	91.04	97.85
	3PT _{su0} (ours)	S	0.95	87.49	22.58	0.55	91.01	83.72
	3PT _{su0} (M) [67]	H [67]	0.86	88.03	558.61	0.53	91.33	1402.46
	3PT _{su0} (ours)	H [67]	0.86	88.03	550.74	0.53	91.33	1392.71

Depth	Solver	Opt.	Mast3r [39]		
			$\epsilon(^{\circ}) \downarrow$	mAA \uparrow	$\tau(ms) \downarrow$
-	5PT [49]	S	0.66	90.29	126.77
Mast3r [39]	Rel3PT [1]	S	0.67	90.30	104.46
	P3P [15]	S	0.67	90.24	56.52
	3PT _{su0} (M) [67]	S	0.67	90.20	42.49
	3PT _{su0} (ours)	S	0.67	90.35	30.90
	3PT _{su0} (M) [67]	H [67]	0.92	87.96	2647.02
	3PT _{su0} (ours)	H [67]	0.92	87.98	2635.27

Table 3. Comparison of different methods on the ETH3D dataset [56] for the calibrated case. Opt.: S - PoseLib [37] implementation using Sampson error, H - hybrid RANSAC from [67].

Solvers: — 3PT_{su0}f(ours) — 3PT_{su0}f(M) [67] — 3p3d [17] — 6PT [26]
 Estimators: — PoseLib [37] — Hybrid [67] — Mast3r [39]

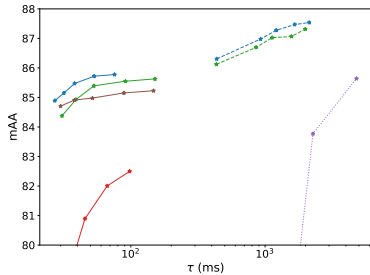


Figure 2. Speed accuracy evaluation for the case of two cameras with shared unknown focal lengths using the RoMA matches [18] and UniDepth [51] depths on the ETH3D dataset [56]. We evaluated mAA and runtimes (τ) for each method running for 50, 100, 200, 500 and 1000 iterations with exception for Mast3r [39] which ran with maximum of 500 iterations.

fast computation is necessary, our solver 3PT_{su0}f implemented in PoseLib [37] performs the best. However, in general, the best accuracy is achieved using the same solver within the hybrid RANSAC scheme [67].

Matches	Depth	Solver	Opt.	$\epsilon(^{\circ}) \downarrow$	$\epsilon_f(^{\circ}) \downarrow$	mAA \uparrow	mAA $f \uparrow$	$\tau(ms) \downarrow$	
SP+LG [14, 42]	Real Depth	6PT [38]	S	2.45	0.04	75.57	61.52	80.02	
		3p3d [17]	S	2.06	0.04	78.00	62.83	30.70	
		4PT _{su0} f(M) [67]	S	1.83	0.03	78.86	63.71	112.34	
		4PT _{su0} f(ours)	S	1.72	0.03	78.90	63.56	51.10	
		3PT _{su0} f(ours)	S	1.75	0.03	79.17	63.63	25.11	
		4PT _{su0} f(M) [67]	H [67]	1.07	0.02	82.01	75.63	1502.02	
	3PT _{su0} f(ours)	H [67]	1.07	0.02	82.19	75.76	1411.05		
	MiDas [8]	3p3d [17]	S	4.08	0.07	61.91	49.69	25.35	
		4PT _{su0} f(M) [67]	S	2.17	0.04	73.99	59.89	103.86	
		4PT _{su0} f(ours)	S	2.26	0.04	73.53	59.35	45.74	
		3PT _{su0} f(ours)	S	2.26	0.04	73.11	60.38	21.36	
		4PT _{su0} f(M) [67]	H [67]	2.58	0.05	68.70	56.01	1303.38	
		3PT _{su0} f(ours)	H [67]	2.47	0.05	69.04	56.45	1316.09	
	DA v2 [66]	3p3d [17]	S	4.54	0.08	61.60	48.76	27.01	
		4PT _{su0} f(M) [67]	S	2.10	0.04	74.60	60.77	104.75	
		4PT _{su0} f(ours)	S	2.02	0.04	74.67	60.41	46.62	
		3PT _{su0} f(ours)	S	2.20	0.04	73.66	60.93	21.62	
		4PT _{su0} f(M) [67]	H [67]	2.34	0.05	70.07	58.00	1190.89	
3PT _{su0} f(ours)		H [67]	2.33	0.05	70.16	58.31	1216.89		
MoGe [62]	3p3d [17]	S	3.18	0.06	68.24	54.64	27.70		
	4PT _{su0} f(M) [67]	S	2.10	0.04	76.06	61.81	107.30		
	4PT _{su0} f(ours)	S	2.15	0.04	75.59	60.88	57.91		
	3PT _{su0} f(ours)	S	1.99	0.04	76.94	62.66	24.72		
	4PT _{su0} f(M) [67]	H [67]	1.50	0.03	79.23	66.34	956.33		
	3PT _{su0} f(ours)	H [67]	1.41	0.03	80.24	67.42	967.52		
UniDepth [51]	3p3d [17]	S	3.49	0.07	69.47	55.57	27.57		
	4PT _{su0} f(M) [67]	S	2.21	0.04	75.61	61.37	106.73		
	4PT _{su0} f(ours)	S	1.92	0.04	76.18	62.00	46.97		
	3PT _{su0} f(ours)	S	2.04	0.04	76.89	62.42	23.47		
	4PT _{su0} f(M) [67]	H [67]	1.27	0.03	81.68	69.64	1107.04		
	3PT _{su0} f(ours)	H [67]	1.28	0.03	81.99	69.28	1149.25		
RoMA [18]	Real Depth	6PT [38]	S	1.15	0.02	85.23	75.03	147.48	
		3p3d [17]	S	0.93	0.02	85.98	74.98	113.30	
		4PT _{su0} f(M) [67]	S	0.99	0.02	86.37	75.21	167.49	
		4PT _{su0} f(ours)	S	1.03	0.02	86.25	75.04	107.05	
		3PT _{su0} f(ours)	S	0.99	0.02	86.68	74.99	79.96	
		4PT _{su0} f(M) [67]	H [67]	2.12	0.02	76.69	72.51	3218.22	
	3PT _{su0} f(ours)	H [67]	2.28	0.02	76.42	72.43	3067.57		
	MiDas [8]	3p3d [17]	S	1.91	0.02	78.71	68.10	86.60	
		4PT _{su0} f(M) [67]	S	1.14	0.02	85.11	74.93	142.78	
		4PT _{su0} f(ours)	S	1.19	0.02	84.86	74.80	84.62	
		3PT _{su0} f(ours)	S	1.25	0.02	84.66	74.47	65.79	
		4PT _{su0} f(M) [67]	H [67]	1.48	0.03	81.10	67.25	2301.37	
		3PT _{su0} f(ours)	H [67]	1.48	0.03	81.44	67.03	2410.90	
	DA v2 [66]	3p3d [17]	S	2.07	0.02	78.86	68.29	91.39	
		4PT _{su0} f(M) [67]	S	1.21	0.02	85.33	75.09	146.35	
		4PT _{su0} f(ours)	S	1.20	0.02	85.61	75.43	88.03	
		3PT _{su0} f(ours)	S	1.23	0.02	84.89	75.00	67.61	
		4PT _{su0} f(M) [67]	H [67]	1.28	0.03	81.56	68.72	2161.36	
3PT _{su0} f(ours)		H [67]	1.30	0.03	81.57	68.68	2245.95		
MoGe [62]	3p3d [17]	S	1.56	0.02	80.98	70.19	98.44		
	4PT _{su0} f(M) [67]	S	1.02	0.02	85.91	75.61	151.65		
	4PT _{su0} f(ours)	S	1.10	0.02	85.85	75.80	92.92		
	3PT _{su0} f(ours)	S	1.05	0.02	86.04	75.83	75.12		
	4PT _{su0} f(M) [67]	H [67]	0.89	0.02	86.99	76.66	1923.31		
	3PT _{su0} f(ours)	H [67]	0.91	0.02	87.20	76.50	2043.91		
UniDepth [51]	3p3d [17]	S	1.89	0.02	82.50	71.89	97.99		
	4PT _{su0} f(M) [67]	S	1.12	0.02	85.63	75.66	151.31		
	4PT _{su0} f(ours)	S	1.12	0.02	85.59	75.64	91.92		
	3PT _{su0} f(ours)	S	1.04	0.02	85.78	75.69	75.62		
	4PT _{su0} f(M) [67]	H [67]	0.83	0.02	87.30	77.34	1997.88		
	3PT _{su0} f(ours)	H [67]	0.82	0.02	87.53	77.79	2133.46		
Mast3r [39]	Mast3r [39]	6PT [38]	S	1.23	0.03	82.99	69.00	85.89	
		3p3d [17]	S	1.37	0.03	81.30	67.31	28.96	
		4PT _{su0} f(M) [67]	S	1.58	0.03	79.68	66.05	95.89	
		4PT _{su0} f(ours)	S	1.36	0.03	80.86	67.16	48.36	
		3PT _{su0} f(ours)	S	1.34	0.03	82.09	68.26	34.54	
		4PT _{su0} f(M) [67]	H [67]	2.43	0.05	72.28	58.32	3825.11	
	3PT _{su0} f(ours)	H [67]	2.39	0.04	72.45	58.61	4079.21		
	-	M [39]	6PT [38]	S	1.32	0.01	85.64	82.95	4800.37

Table 4. Comparison of different methods on the ETH3D dataset [56] for the equal and unknown focal length case. Opt.: S - PoseLib [37] implementation using Sampson error, H - hybrid RANSAC from [67], M - non-linear optimization used in [39].

4.3. Different Focal Lengths

Table 5 shows the comparison of the methods on the Phototourism dataset for two cameras with different unknown focal lengths. As for the previous two cases, when good depth estimate is available the best results are obtained with the hybrid RANSAC scheme [67] in which our solver

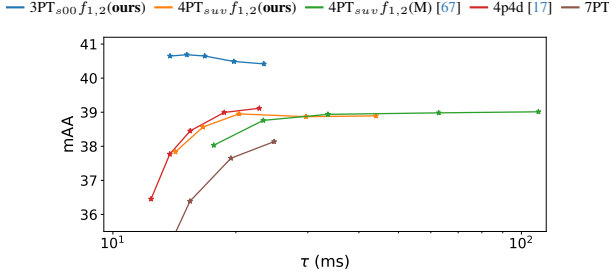


Figure 3. Speed accuracy evaluation for different unknown focal length case using the SP+LG matches [14, 42] and MoGe [62] depths on the Phototourism dataset [30]. We evaluated mAA and runtimes (τ) for each method running for 50, 100, 200, 500 and 1000 iterations within PoseLib [37].

$3PT_{s00}f_{1,2}$ outperforms $4PT_{suv}f_{1,2}(M)$ [67] showing that it is not necessary to model shift for good performance. This is also confirmed by the experiments in PoseLib [37] which show that $3PT_{s00}f$ outperforms other depth-based solvers across all combinations of matches and MDEs in terms of pose accuracy while also being significantly faster than solvers which incorporate shift. Figure 3 shows that $3PT_{s00}f$ clearly outperforms the alternatives in terms of speed and pose estimation accuracy. We observe a slight performance drop in our $3PT_{s00}f$ solver as the number of iterations increases. This may be attributed to the solver converging on physically impossible solutions that yield better scores, such as unrealistic scales or focal lengths. Our current implementation does not include checks to validate the physical feasibility of these parameters (we only consider positive scale and focal length). Incorporating filtering of impossible solutions could be a future work.

Additional Experiments We provide additional experiments in SM which in addition to results on additional datasets also provide evaluation of alternative scoring and LO strategies within PoseLib as well as the proposed $3PT_{100}f$ and $3PT_{100}f_{1,2}$ solvers. We also show that it is possible to use Mast3r [39] for matches in combination with MDE to improve estimated poses and intrinsics.

Limitations. Although using depth maps does not add computational overhead in pose estimation, obtaining these depth maps using learning-based methods introduces additional costs. This is usually a few milliseconds per image [67]. However, in many applications, MDE methods are used for multiple tasks. Thus, the computational overhead is not solely attributable to the pose estimation method.

Compared to standard point-based focal length solvers, the proposed solvers encounter fewer degenerate cases. The formulation allows us to handle pure rotation effectively. However, there are still several degenerate cases similar to those in point-based solvers; for example, four coplanar points and cases of pure translation can introduce degeneracies in focal length recovery [31].

Matches	Depth	Solver	Opt	$\epsilon(^{\circ}) \downarrow$	$\epsilon_f(^{\circ}) \downarrow$	mAA \uparrow	mAA $_f \uparrow$	$\tau(ms) \downarrow$
-	-	7PT [27]	S	8.03	0.17	38.14	23.78	24.80
Real Depth	4p4d [17]	S	S	7.58	0.16	39.34	24.65	23.69
	$4PT_{suv}f_{1,2}(M)$ [67]	S	S	7.33	0.17	39.56	24.08	118.98
	$4PT_{suv}f_{1,2}(\text{ours})$	S	S	7.40	0.17	39.55	24.13	36.71
	$3PT_{s00}f_{1,2}(\text{ours})$	S	S	6.74	0.15	41.25	24.60	25.27
	$4PT_{suv}f_{1,2}(M)$ [67]	H [67]	S	2.86	0.04	63.88	53.46	1922.12
	$3PT_{s00}f_{1,2}(\text{ours})$	H [67]	S	2.82	0.04	64.19	53.73	1901.23
MiDas [8]	4p4d [17]	S	S	12.50	0.24	30.95	18.92	20.67
	$4PT_{suv}f_{1,2}(M)$ [67]	S	S	8.75	0.19	36.60	22.37	112.19
	$4PT_{suv}f_{1,2}(\text{ours})$	S	S	8.91	0.19	36.25	22.18	32.32
	$3PT_{s00}f_{1,2}(\text{ours})$	S	S	8.60	0.19	36.62	21.94	18.17
	$4PT_{suv}f_{1,2}(M)$ [67]	H [67]	S	13.29	0.27	21.68	13.55	2599.72
	$3PT_{s00}f_{1,2}(\text{ours})$	H [67]	S	13.40	0.28	21.33	13.39	2574.24
SP+LG [14, 42]	4p4d [17]	S	S	10.40	0.20	34.72	22.08	22.02
	$4PT_{suv}f_{1,2}(M)$ [67]	S	S	8.17	0.18	37.62	23.32	113.20
	$4PT_{suv}f_{1,2}(\text{ours})$	S	S	8.19	0.18	37.62	23.27	33.14
	$3PT_{s00}f_{1,2}(\text{ours})$	S	S	7.66	0.16	38.90	23.57	20.44
	$4PT_{suv}f_{1,2}(M)$ [67]	H [67]	S	9.55	0.21	32.88	20.88	2490.39
	$3PT_{s00}f_{1,2}(\text{ours})$	H [67]	S	9.48	0.21	32.49	20.65	2494.66
MoGe [62]	4p4d [17]	S	S	7.71	0.16	39.12	24.44	22.82
	$4PT_{suv}f_{1,2}(M)$ [67]	S	S	7.54	0.17	39.01	23.83	110.08
	$4PT_{suv}f_{1,2}(\text{ours})$	S	S	7.65	0.17	38.89	23.85	44.03
	$3PT_{s00}f_{1,2}(\text{ours})$	S	S	7.03	0.16	40.42	24.43	23.41
	$4PT_{suv}f_{1,2}(M)$ [67]	H [67]	S	7.13	0.11	46.38	34.35	857.73
	$3PT_{s00}f_{1,2}(\text{ours})$	H [67]	S	5.90	0.08	49.14	37.80	840.92
UniDepth [51]	4p4d [17]	S	S	7.67	0.16	39.18	24.61	23.63
	$4PT_{suv}f_{1,2}(M)$ [67]	S	S	7.53	0.17	39.25	23.98	118.02
	$4PT_{suv}f_{1,2}(\text{ours})$	S	S	7.55	0.17	39.18	23.99	36.04
	$3PT_{s00}f_{1,2}(\text{ours})$	S	S	7.01	0.15	40.51	24.48	24.61
	$4PT_{suv}f_{1,2}(M)$ [67]	H [67]	S	3.38	0.06	60.15	47.02	1945.50
	$3PT_{s00}f_{1,2}(\text{ours})$	H [67]	S	3.35	0.06	60.38	47.24	1957.65
-	-	7PT [27]	S	4.30	0.10	53.16	34.73	75.10
Real Depth	4p4d [17]	S	S	4.24	0.10	53.51	35.01	77.49
	$4PT_{suv}f_{1,2}(M)$ [67]	S	S	4.22	0.10	54.07	34.83	190.34
	$4PT_{suv}f_{1,2}(\text{ours})$	S	S	4.24	0.10	53.97	34.84	107.46
	$3PT_{s00}f_{1,2}(\text{ours})$	S	S	4.08	0.10	55.22	35.05	100.87
	$4PT_{suv}f_{1,2}(M)$ [67]	H [67]	S	1.60	0.03	75.10	64.07	3518.89
	$3PT_{s00}f_{1,2}(\text{ours})$	H [67]	S	1.58	0.03	75.41	64.37	3531.28
MiDas [8]	4p4d [17]	S	S	5.58	0.13	46.41	29.53	67.95
	$4PT_{suv}f_{1,2}(M)$ [67]	S	S	4.96	0.12	51.13	33.29	164.23
	$4PT_{suv}f_{1,2}(\text{ours})$	S	S	4.91	0.12	51.09	33.08	84.29
	$3PT_{s00}f_{1,2}(\text{ours})$	S	S	4.70	0.11	51.39	32.56	71.37
	$4PT_{suv}f_{1,2}(M)$ [67]	H [67]	S	9.10	0.21	32.05	19.20	4662.34
	$3PT_{s00}f_{1,2}(\text{ours})$	H [67]	S	9.11	0.21	32.04	19.30	4680.00
RoMA [18]	4p4d [17]	S	S	4.61	0.11	51.24	33.30	73.93
	$4PT_{suv}f_{1,2}(M)$ [67]	S	S	4.43	0.10	52.90	34.36	170.68
	$4PT_{suv}f_{1,2}(\text{ours})$	S	S	4.42	0.10	52.83	34.35	90.36
	$3PT_{s00}f_{1,2}(\text{ours})$	S	S	4.20	0.10	53.95	34.56	81.59
	$4PT_{suv}f_{1,2}(M)$ [67]	H [67]	S	6.53	0.16	43.25	27.71	4026.79
	$3PT_{s00}f_{1,2}(\text{ours})$	H [67]	S	6.52	0.16	43.30	27.79	4113.61
MoGe [62]	4p4d [17]	S	S	4.22	0.10	53.61	34.99	77.14
	$4PT_{suv}f_{1,2}(M)$ [67]	S	S	4.33	0.10	53.44	34.72	180.83
	$4PT_{suv}f_{1,2}(\text{ours})$	S	S	4.34	0.10	53.42	34.71	100.14
	$3PT_{s00}f_{1,2}(\text{ours})$	S	S	4.18	0.10	54.49	34.98	95.72
	$4PT_{suv}f_{1,2}(M)$ [67]	H [67]	S	2.56	0.05	68.05	51.63	2096.95
	$3PT_{s00}f_{1,2}(\text{ours})$	H [67]	S	2.50	0.05	68.57	52.03	2158.75
UniDepth [51]	4p4d [17]	S	S	4.20	0.10	53.84	35.24	77.78
	$4PT_{suv}f_{1,2}(M)$ [67]	S	S	4.30	0.10	53.60	34.85	182.14
	$4PT_{suv}f_{1,2}(\text{ours})$	S	S	4.29	0.10	53.53	34.71	99.76
	$3PT_{s00}f_{1,2}(\text{ours})$	S	S	4.18	0.10	54.39	34.91	96.84
	$4PT_{suv}f_{1,2}(M)$ [67]	H [67]	S	2.30	0.04	69.95	53.90	3440.95
	$3PT_{s00}f_{1,2}(\text{ours})$	H [67]	S	2.29	0.04	70.18	54.09	3533.26
-	-	7PT [27]	S	4.39	0.09	54.01	35.02	39.53
Mast3r [39]	4p4d [17]	S	S	5.20	0.11	49.69	31.64	36.90
	$4PT_{suv}f_{1,2}(M)$ [67]	S	S	7.02	0.14	43.95	27.62	108.64
	$4PT_{suv}f_{1,2}(\text{ours})$	S	S	7.03	0.14	44.10	27.81	44.88
	$3PT_{s00}f_{1,2}(\text{ours})$	S	S	5.40	0.12	49.25	30.88	37.40
	$4PT_{suv}f_{1,2}(M)$ [67]	H [67]	S	10.11	0.24	35.16	20.56	4871.24
	$3PT_{s00}f_{1,2}(\text{ours})$	H [67]	S	10.13	0.25	35.17	20.51	4980.42
-	-	M [39]	S	2.71	0.04	66.54	56.43	4903.10

Table 5. Comparison of different methods on the Phototourism dataset [30] for the two unknown focal length case. Opt.: S - PoseLib [37] implementation using Sampson error, H - hybrid RANSAC from [67], M - non-linear optimization used in [39].

5. Conclusion

We address the problem of estimating the relative pose of two cameras using monocular depth predictions. Unlike prior work, which only considered relative depths and their unknown scale factors, we modeled the fact that depth maps can be defined up to unknown scale and shift param-

eters. We propose multiple solvers that jointly estimate the scale, shift (or only one of them), and the relative pose. We consider solvers for calibrated cameras, cameras with shared unknown or different unknown focal lengths. Efficient solvers that outperform state-of-the-art depth-aware solvers are proposed for all three cases. In extensive experiments, we discuss which solvers are preferable in different situations *e.g.* for precise or imprecise depths.

References

- [1] Jonathan Astermark, Yaqing Ding, Viktor Larsson, and Anders Heyden. Fast relative pose estimation using relative depth. In *International Conference on 3D Vision (3DV)*, 2024. 2, 4, 5, 7, 3
- [2] Daniel Barath and Zuzana Kukelova. Relative pose from sift features. In *European Conference on Computer Vision*, pages 454–469. Springer, 2022. 1
- [3] Daniel Barath and Jiří Matas. Graph-cut RANSAC. In *Computer Vision and Pattern Recognition (CVPR)*, 2018. 2, 3
- [4] Daniel Barath and Chris Sweeney. Relative pose solvers using monocular depth. In *2022 26th International Conference on Pattern Recognition (ICPR)*, 2022. 2
- [5] Daniel Barath, Tekla Toth, and Levente Hajder. A minimal solution for two-view focal-length estimation using two affine correspondences. In *Proceedings of the IEEE Conference on Computer Vision and Pattern Recognition*, 2017. 1
- [6] Jacob Bentolila and Joseph M Francos. Conic epipolar constraints from affine correspondences. *Computer Vision and Image Understanding*, 2014. 1
- [7] Shariq Farooq Bhat, Reiner Birkel, Diana Wofk, Peter Wonka, and Matthias Müller. Zoedepth: Zero-shot transfer by combining relative and metric depth. *arXiv preprint arXiv:2302.12288*, 2023. 2, 3
- [8] Reiner Birkel, Diana Wofk, and Matthias Müller. Midas v3. 1—a model zoo for robust monocular relative depth estimation. *arXiv preprint arXiv:2307.14460*, 2023. 2, 3, 6, 7, 8, 4, 5
- [9] Aleksei Bochkovskii, Amaël Delaunoy, Hugo Germain, Marcel Santos, Yichao Zhou, Stephan R Richter, and Vladlen Koltun. Depth pro: Sharp monocular metric depth in less than a second. *arXiv preprint arXiv:2410.02073*, 2024. 1, 2, 3
- [10] Federico Camposco, Andrea Cohen, Marc Pollefeys, and Torsten Sattler. Hybrid Camera Pose Estimation. In *Conference on Computer Vision and Pattern Recognition (CVPR)*, 2018. 3
- [11] Ondřej Chum, Jiří Matas, and Josef Kittler. Locally optimized ransac. In *Pattern Recognition: 25th DAGM Symposium, Magdeburg, Germany, September 10-12, 2003. Proceedings 25*, pages 236–243. Springer, 2003. 6
- [12] David A Cox, John Little, and Donal O’shea. *Using algebraic geometry*. Springer Science & Business Media, 2006. 1, 2
- [13] Angela Dai, Angel X Chang, Manolis Savva, Maciej Halber, Thomas Funkhouser, and Matthias Nießner. Scannet: Richly-annotated 3d reconstructions of indoor scenes. In *Proceedings of the IEEE conference on computer vision and pattern recognition*, 2017. 5, 4, 7
- [14] Daniel DeTone, Tomasz Malisiewicz, and Andrew Rabinovich. Superpoint: Self-supervised interest point detection and description. In *Proceedings of the IEEE conference on computer vision and pattern recognition workshops*, 2018. 6, 7, 8, 3, 4, 5
- [15] Yaqing Ding, Jian Yang, Viktor Larsson, Carl Olsson, and Kalle Åström. Revisiting the p3p problem. In *Computer Vision and Pattern Recognition (CVPR)*, 2023. 4, 5, 6, 7, 3
- [16] Yaqing Ding, Jonathan Astermark, Magnus Oskarsson, and Viktor Larsson. Noisy one-point homographies are surprisingly good. In *Computer Vision and Pattern Recognition (CVPR)*, 2024. 2
- [17] Yaqing Ding, Václav Vávra, Snehal Bhayani, Qianliang Wu, Jian Yang, and Zuzana Kukelova. Fundamental matrix estimation using relative depths. In *European Conference on Computer Vision (ECCV)*, 2024. 2, 3, 4, 5, 7, 8, 6
- [18] Johan Edstedt, Qiyu Sun, Georg Bökman, Márten Wadenbäck, and Michael Felsberg. Roma: Robust dense feature matching. In *Proceedings of the IEEE/CVF Conference on Computer Vision and Pattern Recognition*, 2024. 6, 7, 8, 3, 4, 5
- [19] Ivan Eichhardt and Daniel Barath. Relative pose from deep learned depth and a single affine correspondence. In *European Conference on Computer Vision (ECCV)*, 2020. 1
- [20] Martin A Fischler and Robert C Bolles. Random sample consensus: a paradigm for model fitting with applications to image analysis and automated cartography. *Communications of the ACM*, 1981. 1
- [21] Friedrich Fraundorfer, Petri Tanskanen, and Marc Pollefeys. A minimal case solution to the calibrated relative pose problem for the case of two known orientation angles. In *European Conference on Computer Vision (ECCV)*, 2010. 1
- [22] Xiao-Shan Gao, Xiao-Rong Hou, Jianliang Tang, and Hang-Fei Cheng. Complete solution classification for the perspective-three-point problem. *IEEE transactions on pattern analysis and machine intelligence*, 2003. 4
- [23] Clément Godard, Oisín Mac Aodha, Michael Firman, and Gabriel J Brostow. Digging into self-supervised monocular depth estimation. In *International Conference on Computer Vision (ICCV)*, 2019. 1
- [24] Daniel R. Grayson and Michael E. Stillman. Macaulay2, a software system for research in algebraic geometry. Available at <http://www2.macaulay2.com>, 1992. 2
- [25] Banglei Guan and Ji Zhao. Relative pose estimation for multi-camera systems from point correspondences with scale ratio. In *Proceedings of the 30th ACM International Conference on Multimedia*, 2022. 1, 2
- [26] Richard Hartley and Hongdong Li. An efficient hidden variable approach to minimal-case camera motion estimation. *Trans. Pattern Analysis and Machine Intelligence (PAMI)*, 2012. 1, 4, 7
- [27] Richard Hartley and Andrew Zisserman. *Multiple view geometry in computer vision*. Cambridge university press, 2003. 1, 2, 4, 5, 8, 6, 7

- [28] Mu Hu, Wei Yin, Chi Zhang, Zhipeng Cai, Xiaoxiao Long, Hao Chen, Kaixuan Wang, Gang Yu, Chunhua Shen, and Shaojie Shen. Metric3d v2: A versatile monocular geometric foundation model for zero-shot metric depth and surface normal estimation. *arXiv preprint arXiv:2404.15506*, 2024. 1, 2, 3
- [29] Kaiwen Jiang, Yang Fu, Mukund Varma T, Yash Belhe, Xiaolong Wang, Hao Su, and Ravi Ramamoorthi. A construct-optimize approach to sparse view synthesis without camera pose. In *ACM SIGGRAPH 2024 Conference Papers*, 2024. 2
- [30] Yuhe Jin, Dmytro Mishkin, Anastasiia Mishchuk, Jiri Matas, Pascal Fua, Kwang Moo Yi, and Eduard Trulls. Image Matching across Wide Baselines: From Paper to Practice. *International Journal of Computer Vision*, 2020. 5, 6, 8, 4
- [31] Fredrik Kahl and Bill Triggs. Critical motions in euclidean structure from motion. In *Computer Vision and Pattern Recognition (CVPR)*, 1999. 8
- [32] Bingxin Ke, Anton Obukhov, Shengyu Huang, Nando Metzger, Rodrigo Caye Daudt, and Konrad Schindler. Repurposing diffusion-based image generators for monocular depth estimation. In *Proceedings of the IEEE/CVF Conference on Computer Vision and Pattern Recognition (CVPR)*, 2024. 2, 3
- [33] Viktor Kocur, Daniel Kyselica, and Zuzana Kukelova. Robust self-calibration of focal lengths from the fundamental matrix. In *Proceedings of the IEEE/CVF Conference on Computer Vision and Pattern Recognition*, pages 5220–5229, 2024. 6
- [34] Zuzana Kukelova, Martin Bujnak, and Tomas Pajdla. Closed-form solutions to minimal absolute pose problems with known vertical direction. In *Asian Conference on Computer Vision (ACCV)*, 2010. 1
- [35] Zuzana Kukelova, Martin Bujnak, and Tomas Pajdla. Polynomial eigenvalue solutions to minimal problems in computer vision. *Trans. Pattern Analysis and Machine Intelligence (PAMI)*, 2012. 1, 2
- [36] Zuzana Kukelova, Joe Kileel, Bernd Sturmfels, and Tomas Pajdla. A clever elimination strategy for efficient minimal solvers. In *Computer Vision and Pattern Recognition (CVPR)*, 2017. 1
- [37] Viktor Larsson and contributors. PoseLib - Minimal Solvers for Camera Pose Estimation, 2020. 6, 7, 8, 3, 4, 5
- [38] Viktor Larsson, Kalle Åström, and Magnus Oskarsson. Efficient solvers for minimal problems by syzygy-based reduction. In *Computer Vision and Pattern Recognition (CVPR)*, 2017. 5, 7, 2
- [39] Vincent Leroy, Yohann Cabon, and Jérôme Revaud. Grounding image matching in 3d with mast3r. In *European Conference on Computer Vision*. Springer, 2024. 2, 6, 7, 8, 3, 4, 5
- [40] Jiahe Li, Jiawei Zhang, Xiao Bai, Jin Zheng, Xin Ning, Jun Zhou, and Lin Gu. Dngaussian: Optimizing sparse-view 3d gaussian radiance fields with global-local depth normalization. In *Proceedings of the IEEE/CVF conference on computer vision and pattern recognition*, 2024. 2
- [41] Hyon Lim, Sudipta N. Sinha, Michael F. Cohen, Matt Uyttendaele, and H. Jin Kim. Real-time Monocular Image-based 6-DoF Localization. *IJRR*, 34(4–5):476–492, 2015. 1
- [42] Philipp Lindenberger, Paul-Edouard Sarlin, and Marc Pollefeys. Lightglue: Local feature matching at light speed. In *International Conference on Computer Vision (ICCV)*, 2023. 6, 7, 8, 3, 4, 5
- [43] Sheng Liu, Xiaohan Nie, and Raffay Hamid. Depth-guided sparse structure-from-motion for movies and tv shows. In *Proceedings of the IEEE/CVF Conference on Computer Vision and Pattern Recognition*, 2022. 2
- [44] Stephan Liwicki and Christopher Zach. Scale exploiting minimal solvers for relative pose with calibrated cameras. In *BMVC*, 2017. 1, 2
- [45] David G Lowe. Distinctive image features from scale-invariant keypoints. *International journal of computer vision*, 60(2):91–110, 2004. 2
- [46] Gonzalo Martin Garcia, Karim Abou Zeid, Christian Schmidt, Daan de Geus, Alexander Hermans, and Bastian Leibe. Fine-tuning image-conditional diffusion models is easier than you think, 2024. 1, 2, 3
- [47] Nathaniel Merrill, Patrick Geneva, Saimouli Katragadda, Chuchu Chen, and Guoquan Huang. Fast monocular visual-inertial initialization leveraging learned single-view depth. *Robotics: Science and Systems (RSS) 2023*, 2023. 2
- [48] Oleg Naroditsky, Xun S Zhou, Jean Gallier, Stergios I Roumeliotis, and Kostas Daniilidis. Two efficient solutions for visual odometry using directional correspondence. *Trans. Pattern Analysis and Machine Intelligence (PAMI)*, 2012. 1
- [49] David Nistér. An efficient solution to the five-point relative pose problem. *Trans. Pattern Analysis and Machine Intelligence (PAMI)*, 2004. 1, 2, 3, 4, 5, 7
- [50] Mikael Persson and Klas Nordberg. Lambda twist: An accurate fast robust perspective three point (p3p) solver. In *Proceedings of the European conference on computer vision (ECCV)*, pages 318–332, 2018. 4
- [51] Luigi Piccinelli, Yung-Hsu Yang, Christos Sakaridis, Mattia Segu, Siyuan Li, Luc Van Gool, and Fisher Yu. Unidepth: Universal monocular metric depth estimation. In *Proceedings of the IEEE/CVF Conference on Computer Vision and Pattern Recognition*, pages 10106–10116, 2024. 1, 2, 3, 6, 7, 8, 4, 5
- [52] René Ranftl, Alexey Bochkovskiy, and Vladlen Koltun. Vision transformers for dense prediction. In *International Conference on Computer Vision (ICCV)*, 2021. 2, 3
- [53] Paul-Edouard Sarlin, Cesar Cadena, Roland Siegwart, and Marcin Dymczyk. From coarse to fine: Robust hierarchical localization at large scale. In *Computer Vision and Pattern Recognition (CVPR)*, 2019. 1, 6
- [54] Paul-Edouard Sarlin, Daniel DeTone, Tomasz Malisiewicz, and Andrew Rabinovich. Superglue: Learning feature matching with graph neural networks. In *Proceedings of the IEEE/CVF conference on computer vision and pattern recognition*, 2020. 5
- [55] Johannes L Schonberger and Jan-Michael Frahm. Structure-from-motion revisited. In *Computer Vision and Pattern Recognition (CVPR)*, pages 4104–4113, 2016. 1
- [56] Thomas Schops, Johannes L Schonberger, Silvano Galliani, Torsten Sattler, Konrad Schindler, Marc Pollefeys, and Andreas Geiger. A multi-view stereo benchmark with high-

- resolution images and multi-camera videos. In *Computer Vision and Pattern Recognition (CVPR)*, 2017. 5, 6, 7, 3
- [57] Henrik Stewénus, David Nistér, Fredrik Kahl, and Frederik Schaffalitzky. A minimal solution for relative pose with unknown focal length. In *Computer Vision and Pattern Recognition (CVPR)*, 2005. 1
- [58] Henrik Stewénus, Christopher Engels, and David Nistér. Recent developments on direct relative orientation. *ISPRS Journal of Photogrammetry and Remote Sensing*, 60(4):284–294, 2006. 1, 2
- [59] Linus Svärm, Olof Enqvist, Fredrik Kahl, and Magnus Oskarsson. City-scale localization for cameras with known vertical direction. *Trans. Pattern Analysis and Machine Intelligence (PAMI)*, 2016. 1
- [60] Chris Sweeney, John Flynn, and Matthew Turk. Solving for relative pose with a partially known rotation is a quadratic eigenvalue problem. *International Conference on 3D Vision (3DV)*, 2014. 1
- [61] Philip HS Torr and Andrew Zisserman. Mlesac: A new robust estimator with application to estimating image geometry. *Computer vision and image understanding*, 2000. 3
- [62] Ruicheng Wang, Sicheng Xu, Cassie Dai, Jianfeng Xiang, Yu Deng, Xin Tong, and Jiaolong Yang. Moge: Unlocking accurate monocular geometry estimation for open-domain images with optimal training supervision, 2024. 1, 2, 3, 6, 7, 8, 4, 5
- [63] Shuzhe Wang, Vincent Leroy, Yohann Cabon, Boris Chidlovskii, and Jerome Revaud. Dust3r: Geometric 3d vision made easy. In *Proceedings of the IEEE/CVF Conference on Computer Vision and Pattern Recognition*, 2024. 2, 6
- [64] Chen Yang, Sikuang Li, Jiemin Fang, Ruofan Liang, Lingxi Xie, Xiaopeng Zhang, Wei Shen, and Qi Tian. Gaussianobject: High-quality 3d object reconstruction from four views with gaussian splatting. *ACM Transactions on Graphics (TOG)*, 2024. 2
- [65] Lihe Yang, Bingyi Kang, Zilong Huang, Xiaogang Xu, Jiashi Feng, and Hengshuang Zhao. Depth anything: Unleashing the power of large-scale unlabeled data. In *Computer Vision and Pattern Recognition (CVPR)*, 2024. 1, 2, 3
- [66] Lihe Yang, Bingyi Kang, Zilong Huang, Zhen Zhao, Xiaogang Xu, Jiashi Feng, and Hengshuang Zhao. Depth anything v2. *arXiv preprint arXiv:2406.09414*, 2024. 1, 2, 3, 6, 7, 8, 4, 5
- [67] Yifan Yu, Shaohui Liu, Rémi Pautrat, Marc Pollefeys, and Viktor Larsson. Relative pose estimation through affine corrections of monocular depth priors. *arXiv preprint arXiv:2501.05446*, 2025. 2, 3, 4, 5, 6, 7, 8
- [68] Zehao Yu, Songyou Peng, Michael Niemeyer, Torsten Sattler, and Andreas Geiger. Monosdf: Exploring monocular geometric cues for neural implicit surface reconstruction. *Advances in neural information processing systems*, 2022. 2
- [69] Bernhard Zeisl, Torsten Sattler, and Marc Pollefeys. Camera pose voting for large-scale image-based localization. In *International Conference on Computer Vision (ICCV)*, 2015. 1
- [70] Yunwen Zhou, Abhishek Kar, Eric Turner, Adarsh Kowdle, Chao X Guo, Ryan C DuToit, and Konstantine Tsotsos.

Learned monocular depth priors in visual-inertial initialization. In *European conference on computer vision*, 2022. 2

RePoseD: Efficient Relative Pose Estimation With Known Depth Information

Supplementary Material

This supplementary material provides the following information: Sec. 6 provides more details about the proposed solvers, including a general approach that can be used to solve all variants of the depth-aware relative pose problem that require 3 point correspondences, the 3PT_{*su*v}(inverse) solver for affine-invariant inverse depths, and the variants of the affine-invariant 4PT focal length solvers. Sec. 7 provides more experimental results.

6. More Details About the Solvers

6.1. Solvers Using Three Point Correspondences

For calibrated camera pose estimation with monocular depth, all possible cases can be solved using three point correspondences and a varying number of monocular depth estimates. Similarly, for focal length problems, most cases can be solved using three point correspondences and a varying number of depth estimates. In general, all cases that involve three point correspondences can be solved using a similar approach.

Here we show the solution to the shared unknown focal length scale-invariant case, *i.e.* the 3PT_{*s00f*} solver. In this case, the shifts in the monocular depths are omitted (considered to be zero) and we only consider the unknown scales. The minimal case is two 3D-3D point correspondence with one 3D-2D point correspondences. We have

$$\begin{aligned} \|s\mathbf{K}^{-1}(\beta_1\mathbf{q}_1 - \beta_2\mathbf{q}_2)\| &= \|\mathbf{K}^{-1}(\alpha_1\mathbf{p}_1 - \alpha_2\mathbf{p}_2)\|, \\ \|s\mathbf{K}^{-1}(\beta_1\mathbf{q}_1 - \eta_3\mathbf{q}_3)\| &= \|\mathbf{K}^{-1}(\alpha_1\mathbf{p}_1 - \alpha_3\mathbf{p}_3)\|, \\ \|s\mathbf{K}^{-1}(\beta_2\mathbf{q}_2 - \eta_3\mathbf{q}_3)\| &= \|\mathbf{K}^{-1}(\alpha_2\mathbf{p}_2 - \alpha_3\mathbf{p}_3)\|. \end{aligned}$$

where $\alpha_1, \alpha_2, \alpha_3, \beta_1, \beta_2$ are known depths estimated *e.g.* using MDE network, and η_3 is the unknown depth.³ There are three equations in three unknowns $\{s, f, \eta_3\}$, which can be solved similarly as for the 3PT_{*su*v} solver presented in Sec. 3.1 of the main paper. In general, all the problems using three point correspondences can be converted into solving three equations in three unknowns. They differ in the number of depth parameters for the 2D points, but the structure and the solution strategy in all cases similar.

6.2. 3PT_{*su*v} Inverse Depth Solver

Some MDE networks return affine-invariant inverse depths. In this case, the true depths can be expressed as

$$\eta_i = \frac{s_1}{\alpha_i + u}, \quad \lambda_i = \frac{s_2}{\beta_i + v}, \quad (6)$$

³Note that in this case, for the last (third) correspondence, we assume that we know/use the depth only from one image, *i.e.* we have 3D-2D correspondence with unknown depth η_3 .

where α_i, β_i are known values from the inverse monocular depth, and $\{s_1, s_2\}, \{u, v\}$ are the unknown scales and shifts in the inverse depth. In this case, we have

$$\frac{s_2}{\beta_i + v}\mathbf{K}_2^{-1}\mathbf{q}_i = \frac{s_1}{\alpha_i + u}\mathbf{R}\mathbf{K}_1^{-1}\mathbf{p}_i + \mathbf{T}, \quad (7)$$

Dividing (7) by s_1 gives

$$\frac{s}{\beta_i + v}\mathbf{K}_2^{-1}\mathbf{q}_i = \frac{1}{\alpha_i + u}\mathbf{R}\mathbf{K}_1^{-1}\mathbf{p}_i + \mathbf{t}, \quad (8)$$

In this case, similarly to the affine-invariant depth case, we have 9 DOF for calibrated cameras. However, in contrast to the affine-invariant depths, the constraints (8) for affine-invariant inverse depths are more complicated, since they contain unknown parameters in the denominators. We can use similar tricks to eliminate the rotation and translation from the original equations (8) as the ones used for the affine-invariant depth solvers presented in the main paper. In this case, we obtain

$$\begin{aligned} \left\| \frac{s\tilde{\mathbf{q}}_1}{\beta_1 + v} - \frac{s\tilde{\mathbf{q}}_2}{\beta_2 + v} \right\| &= \left\| \frac{\tilde{\mathbf{p}}_1}{\alpha_1 + u} - \frac{\tilde{\mathbf{p}}_2}{\alpha_2 + u} \right\|, \\ \left\| \frac{s\tilde{\mathbf{q}}_1}{\beta_1 + v} - \frac{s\tilde{\mathbf{q}}_3}{\beta_3 + v} \right\| &= \left\| \frac{\tilde{\mathbf{p}}_1}{\alpha_1 + u} - \frac{\tilde{\mathbf{p}}_3}{\alpha_3 + u} \right\|, \\ \left\| \frac{s\tilde{\mathbf{q}}_2}{\beta_2 + v} - \frac{s\tilde{\mathbf{q}}_3}{\beta_3 + v} \right\| &= \left\| \frac{\tilde{\mathbf{p}}_2}{\alpha_2 + u} - \frac{\tilde{\mathbf{p}}_3}{\alpha_3 + u} \right\|. \end{aligned} \quad (9)$$

However, these equations have unknowns in the denominators, and simply multiplying the equations with the denominators results in a very complex system of equations that is difficult to solve.

To solve the equations efficiently, we first multiply (9) with $\alpha_1 + u$, and let

$$\begin{aligned} b_1 &= \frac{s(\alpha_1 + u)}{\beta_1 + v}, \quad b_2 = \frac{s(\alpha_1 + u)}{\beta_2 + v}, \quad b_3 = \frac{s(\alpha_1 + u)}{\beta_3 + v}, \\ c_2 &= \frac{\alpha_1 + u}{\alpha_2 + u}, \quad c_3 = \frac{\alpha_1 + u}{\alpha_3 + u}. \end{aligned} \quad (10)$$

Substituting (10) into (9) we have three equations

$$\begin{aligned} \|b_1\tilde{\mathbf{q}}_1 - b_2\tilde{\mathbf{q}}_2\| &= \|\tilde{\mathbf{p}}_1 - c_2\tilde{\mathbf{p}}_2\|, \\ \|b_1\tilde{\mathbf{q}}_1 - b_3\tilde{\mathbf{q}}_3\| &= \|\tilde{\mathbf{p}}_1 - c_3\tilde{\mathbf{p}}_3\|, \\ \|b_2\tilde{\mathbf{q}}_2 - b_3\tilde{\mathbf{q}}_3\| &= \|c_2\tilde{\mathbf{p}}_2 - c_3\tilde{\mathbf{p}}_3\|, \end{aligned} \quad (11)$$

where b_1, b_2, b_3, c_2, c_3 are new unknowns. However, these unknown are not independent. To find the constraints on b_1, b_2, b_3, c_2, c_3 , we use the elimination ideal technique [12]. In this case, we first create an ideal J generated by five polynomials (10). Then, the unknown parameters s, u, v are eliminated from the generators of J

by computing the generators of the elimination ideal $J_1 = J \cap \mathbb{C}[\alpha_1, \alpha_2, \dots, c_2, c_3]$. These generators can be computed using the following Macaulay2 [24] code

```
R = QQ[s, u, v, alpha_1, alpha_2, alpha_3, beta_1, beta_2, beta_3, b_1, b_2, b_3, c_2, c_3];
eq = {b_1(beta_1 + v) - s(alpha_1 + u), b_2(beta_2 + v) - s(alpha_1 + u),
      b_3(beta_3 + v) - s(alpha_1 + u), c_2(alpha_2 + u) - (alpha_1 + u),
      c_3(alpha_3 + u) - (alpha_1 + u)};
J = ideal(eq);
J1 = eliminate(J, {s, u, v});
g = mingens J1;
"constraints.txt" << toString g << close;
```

In this case, by eliminating $\{s, u, v\}$ from (10) we obtain the following two equations in $\{b_1, b_2, b_3, c_2, c_3\}$

$$\begin{aligned} b_1 b_2 \beta_1 - b_1 b_3 \beta_1 - b_1 b_2 \beta_2 + b_2 b_3 \beta_2 + b_1 b_3 \beta_3 - b_2 b_3 \beta_3 &= 0, \\ c_2 c_3 \alpha_2 - c_2 c_3 \alpha_3 + c_2 \alpha_1 - c_3 \alpha_1 - c_2 \alpha_2 + c_3 \alpha_3 &= 0. \end{aligned} \quad (12)$$

Combining (12) with (11) we have 5 equations in 5 unknowns, which can be solved using the Gröbner basis method [12]. Using the automatic generator of Gröbner basis solvers [38], we obtain a solver with an elimination template of size 54×66 and 12 solutions. Note that there are two trivial solutions $b_2 = b_3 = c_2 = c_3 = 0$, $\|b_1 \tilde{q}_1\| = \|\tilde{p}_1\|$. Hence, there are up to 10 feasible solutions.

The $3PT_{suv}$ (inverse) solver is much more complex than the $3PT_{suv}$ solver for affine-invariant depths presented in the main paper. In the next section, we show that the $3PT_{suv}$ (inverse) solver does not give better results than the $3PT_{suv}$ solver inside RANSAC even when used with affine-invariant inverse depths.

6.3. Fast 4PT Solvers

In Sec 3.2 of the main paper, we have mentioned that the focal length problems with affine-invariant depth can be efficiently solved using all the six equations. Here we provide more details on the solutions.

4PT_{suv}f(Eigen). By using four 3D-3D point correspondences, we can rewrite the six equations for this problem as

$$\mathbf{M} [1, c, cv, cv^2, u, u^2, f^2, cf^2]^\top = 0, \quad (13)$$

where \mathbf{M} is a 6×8 coefficient matrix.

Since these equations only contain f^2 , we let $w = f^2$ and consider w as the hidden variable [35]. Then (13) can be written as

$$\mathbf{M}(w) [1, c, cv, cv^2, u, u^2]^\top = 0, \quad (14)$$

where $\mathbf{M}(w)$ is a 6×6 polynomial matrix in w . In this case

$$\mathbf{M}(w) = \mathbf{M}_0 + w\mathbf{M}_1, \quad (15)$$

where \mathbf{M}_0 and \mathbf{M}_1 are 6×6 coefficient matrices.

Thus, in this case, the solutions to $1/w$ are the eigenvalues of the following matrix

$$\mathbf{A} = -\mathbf{M}_0^{-\top} \mathbf{M}_1^\top. \quad (16)$$

Note that there are 4 zero columns in \mathbf{M}_1 , which will result in zero eigenvalues. Based on [35], these zero columns can be removed together with the zero rows. Hence, we only need to find the eigenvalues of a 2×2 matrix resulting in 2 solutions to the problem. We denote this solver as $4PT_{suv}f$ (Eigen).

4PT_{suv}f_{1,2}(Eigen). For different and unknown focal lengths case, we have the following six equations

$$\mathbf{m}_i [1, c, cf_2^2, cf_2^2 v, cf_2^2 v^2, f_1^2, f_1^2 u, f_1^2 u^2]^\top = 0, \quad (17)$$

where $i = 1, 2, \dots, 6$. We consider v as a hidden variable, and (17) can be written as

$$\mathbf{M}(v) [1, c, cf_2^2, f_1^2, f_1^2 u, f_1^2 u^2]^\top = 0, \quad (18)$$

where $\mathbf{M}(v)$ is a 6×6 polynomial matrix in v . It can be solved similarly to the shared unknown focal length case, and there are only two possible solutions. We denote this solver as $4PT_{suv}f_{1,2}$ (Eigen).

7. More Experiments

7.1. Results for 3PT_{suv}(Inverse)

This solver was derived to be used with affine-invariant inverse depths, *e.g.*, obtained via Depth Anything [65]. However, we observed that the $3PT_{suv}$ (inverse) solver does not improve the accuracy even for affine-invariant inverse depths when used inside RANSAC. In addition, $3PT_{suv}$ (inverse) is much more time-consuming than the $3PT_{suv}$ solver as shown in Table 6. In this experiment, we use GC-RANSAC [3] without LO to show that $3PT_{suv}$ (inverse) solver is not practical. As such, we did not evaluate the $3PT_{suv}$ (inverse) solver in the main paper.

Depth	Method	Phototourism				
		$\epsilon_R(^{\circ}) \downarrow$	$\epsilon_t(^{\circ}) \downarrow$	mAA(R) \uparrow	mAA(t) \uparrow	$\tau(ms) \downarrow$
DA V2 [66]	$3PT_{suv}$	1.27	2.94	0.83	0.66	45.37
	$3PT_{suv}$ (inverse)	1.28	3.02	0.83	0.65	194.77

Table 6. Comparison between $3PT_{suv}$ and $3PT_{suv}$ (inverse) using Depth anything V2 [66] on the Phototourism dataset with GC-RANSAC [3].

7.2. Results for Fast 4PT Solvers

Table 7 shows that the relaxed eigenvalue solvers for the focal length problems are faster but give much worse results. Hence, we didn't use them in the real experiments.

7.3. More Results

We provide more results for the three different cases including more datasets, RANSAC configurations, and additional solvers. Tables 8-10 show results for the calibrated case

Depth	Method	Phototourism						
		$\epsilon_R(^{\circ}) \downarrow$	$\epsilon_t(^{\circ}) \downarrow$	$\epsilon_f \downarrow$	mAA(R) \uparrow	mAA(t) \uparrow	mAA(f) \uparrow	$\tau(ms) \downarrow$
DA V2 [66]	4PT _{suvs} f	2.32	6.58	0.22	0.72	0.44	0.33	50.99
	4PT _{suvs} f(Eigen)	5.17	17.25	0.30	0.52	0.22	0.21	8.18
	4PT _{suvs} f _{1,2}	5.78	17.37	0.26	0.48	0.20	0.23	54.27
	4PT _{suvs} f _{1,2} (Eigen)	7.65	23.42	0.32	0.39	0.15	0.18	7.92

Table 7. Comparison between the focal length solvers shown in the main paper and the fast eigenvalue solutions inside GC-RANSAC [3].

for the ETH3D, Phototourism and ScanNet datasets respectively. We note that Mast3r [39] with its non-linear optimization strategy is not included for the calibrated case, since the authors recommend using the 5PT [49] solver with RANSAC to obtain the poses instead. Tables 11 and 12 show results for shared focal length case for the ETH3D and ScanNet datasets. Tables 13-15 show results for different unknown focal length case for the ETH3D, Phototourism and ScanNet datasets respectively.

Tables 8-15 include an alternative configuration of PoseLib [37] in which we use the reprojection error for scoring and LO denoted as R or its version with included shift denoted as R_s. Using this strategy generally does not produce improvements over using the Sampson error. However, we note that for ScanNet using the reprojection error outperforms Sampson error when the estimated depth is accurate. This may be due to the fact that ScanNet contains only indoor scenes, and thus depth estimates may be more reliable.

We have also evaluated our proposed solvers 3PT₁₀₀f and 3PT₁₀₀f_{1,2} for the shared and different unknown focal cases respectively. These solvers assume zero shifts and known scales or same scales in both images and thus known scale ratio s . On Phototourism and ETH3D they perform worse than alternatives. However, when evaluated on ScanNet these solvers perform on par with solvers considering scale and shift. Additionally, solvers that do not model scale and shift can still produce reasonable results when using Mast3r’s depth, as Mast3r inherently corrects depth scales based on multi-view information. This suggests that in some scenarios (such as indoor scenes) MDEs may provide depths for which scale and shift do not need to be considered.

For the case of different focal lengths on the ScanNet dataset Mast3r [39] with its optimization strategy achieves the best results. However, we show that these results can be surpassed when Mast3r matches are used in conjunction with MoGe [62] for depth estimation. For this combination, the hybrid RANSAC strategy [67] with either of the evaluated solvers yields better accuracy in both pose and focal length than Mast3r. We note that the runtime evaluation is fair, since for Mast3r runtime we do not include the inference time of the network which produces the matches.

Depth	Solver	Opt.	SP+LG [14, 42]			RoMA [18]		
			$\epsilon(^{\circ}) \downarrow$	mAA \uparrow	$\tau(ms) \downarrow$	$\epsilon(^{\circ}) \downarrow$	mAA \uparrow	$\tau(ms) \downarrow$
Real Depth	5PT [49]	S	0.91	87.67	48.14	0.56	91.10	184.36
	Rel3PT [1]	S	0.88	88.21	103.18	0.52	91.38	532.02
	P3P [15]	S	0.83	88.88	29.68	0.52	91.33	141.39
	3PT _{suvs} (M) [67]	S	0.79	88.55	41.81	0.45	91.39	145.59
	3PT _{suvs} (ours)	S	0.80	88.60	29.59	0.47	91.37	127.81
	P3P [15]	R	0.33	92.56	13.27	0.26	93.41	52.53
	3PT _{suvs} (M) [67]	R	0.32	92.60	25.64	0.25	93.91	57.20
	3PT _{suvs} (ours)	R	0.32	92.57	13.76	0.25	93.90	42.86
	P3P [15]	R _s	0.36	92.30	14.47	0.29	93.33	57.28
	3PT _{suvs} (M) [67]	R _s	0.36	92.12	26.70	0.29	93.46	62.30
	3PT _{suvs} (ours)	R _s	0.36	92.10	15.27	0.29	93.46	45.96
	3PT _{suvs} (M) [67]	H [67]	0.52	91.39	549.59	0.39	92.73	1505.19
	3PT _{suvs} (ours)	H [67]	0.52	91.42	543.48	0.39	92.72	1490.93
	MiDas [8]	Rel3PT [1]	S	4.81	71.25	36.34	3.23	82.22
P3P [15]		S	0.94	86.16	22.97	0.60	90.80	91.36
3PT _{suvs} (M) [67]		S	0.88	87.34	31.11	0.58	90.77	79.17
3PT _{suvs} (ours)		S	0.88	87.39	20.40	0.59	90.76	67.13
P3P [15]		R	12.40	28.75	14.86	9.06	37.21	65.21
3PT _{suvs} (M) [67]		R	12.16	28.56	23.87	9.17	37.19	53.98
3PT _{suvs} (ours)		R	12.24	28.61	13.25	9.30	36.91	42.72
P3P [15]		R _s	8.05	38.57	14.60	6.00	48.28	57.97
3PT _{suvs} (M) [67]		R _s	5.68	49.47	24.18	3.75	63.57	48.37
3PT _{suvs} (ours)		R _s	5.69	49.64	13.79	3.75	63.54	37.26
3PT _{suvs} (M) [67]		H [67]	1.08	85.38	685.32	0.67	90.49	1605.43
3PT _{suvs} (ours)		H [67]	1.07	85.45	683.39	0.67	90.50	1590.71
Rel3PT [1]		S	5.57	68.46	35.74	3.90	80.56	145.85
P3P [15]		S	0.90	86.25	23.26	0.72	90.61	93.99
3PT _{suvs} (M) [67]	S	0.90	87.19	32.50	0.56	90.99	88.60	
3PT _{suvs} (ours)	S	0.91	87.07	21.68	0.56	91.01	75.87	
P3P [15]	R	11.40	30.75	14.88	9.31	37.43	65.83	
3PT _{suvs} (M) [67]	R	11.73	30.08	24.46	9.19	37.18	56.91	
3PT _{suvs} (ours)	R	11.71	29.93	13.52	9.20	37.25	45.22	
P3P [15]	R _s	6.87	43.36	14.71	5.12	52.28	59.11	
3PT _{suvs} (M) [67]	R _s	4.24	56.53	24.89	2.69	68.58	53.70	
3PT _{suvs} (ours)	R _s	4.27	56.50	14.13	2.70	68.50	42.35	
3PT _{suvs} (M) [67]	H [67]	0.97	85.52	605.63	0.54	90.62	1493.75	
3PT _{suvs} (ours)	H [67]	0.98	85.56	593.95	0.54	90.62	1477.73	
MoGe [62]	Rel3PT [1]	S	4.74	72.08	42.19	2.74	82.04	170.29
	P3P [15]	S	0.91	87.67	25.72	0.54	91.16	111.74
	3PT _{suvs} (M) [67]	S	0.89	87.71	33.45	0.53	91.04	98.20
	3PT _{suvs} (ours)	S	0.89	87.67	22.41	0.54	91.05	84.24
	P3P [15]	R	1.89	77.65	15.16	1.48	83.13	66.70
	3PT _{suvs} (M) [67]	R	1.90	77.43	24.49	1.48	83.11	57.53
	3PT _{suvs} (ours)	R	1.92	77.31	13.45	1.47	83.13	45.41
	P3P [15]	R _s	1.68	79.07	15.51	1.28	84.99	64.68
	3PT _{suvs} (M) [67]	R _s	1.76	78.13	24.93	1.32	84.91	55.70
	3PT _{suvs} (ours)	R _s	1.77	78.07	14.12	1.31	84.99	43.77
	3PT _{suvs} (M) [67]	H [67]	0.86	88.26	566.16	0.50	91.17	1414.96
	3PT _{suvs} (ours)	H [67]	0.85	88.24	554.79	0.49	91.23	1401.61
	Rel3PT [1]	S	1.36	78.82	49.70	0.70	88.25	207.86
	P3P [15]	S	0.88	88.00	25.93	0.56	91.11	112.65
3PT _{suvs} (M) [67]	S	0.94	87.42	33.90	0.55	91.04	97.85	
3PT _{suvs} (ours)	S	0.95	87.49	22.58	0.55	91.01	83.72	
P3P [15]	R	2.02	76.60	15.48	1.59	82.49	68.16	
3PT _{suvs} (M) [67]	R	2.05	76.28	24.68	1.57	82.38	58.47	
3PT _{suvs} (ours)	R	2.05	76.17	13.63	1.59	82.30	46.47	
P3P [15]	R _s	1.78	78.26	15.64	1.29	84.85	64.83	
3PT _{suvs} (M) [67]	R _s	1.80	77.51	25.03	1.31	84.93	55.43	
3PT _{suvs} (ours)	R _s	1.81	77.40	14.18	1.30	84.98	43.64	
3PT _{suvs} (M) [67]	H [67]	0.86	88.03	558.61	0.53	91.33	1402.46	
3PT _{suvs} (ours)	H [67]	0.86	88.03	550.74	0.53	91.33	1392.71	

Depth	Solver	Opt.	Mast3r [39]		
			$\epsilon(^{\circ}) \downarrow$	mAA \uparrow	$\tau(ms) \downarrow$
-	5PT [49]	S	0.66	90.29	126.77
Mast3r [39]	Rel3PT [1]	S	0.67	90.30	104.46
	P3P [15]	S	0.67	90.24	56.52
	3PT _{suvs} (M) [67]	S	0.67	90.20	42.49
	3PT _{suvs} (ours)	S	0.67	90.35	30.90
	P3P [15]	R	29.42	17.49	38.12
	3PT _{suvs} (M) [67]	R	29.98	16.85	33.80
	3PT _{suvs} (ours)	R	30.00	17.05	22.95
	P3P [15]	R _s	23.13	18.65	36.68
	3PT _{suvs} (M) [67]	R _s	23.74	15.23	31.22
	3PT _{suvs} (ours)	R _s	24.16	14.97	21.01
	3PT _{suvs} (M) [67]	H [67]	0.92	87.96	2647.02
3PT _{suvs} (ours)	H [67]	0.92	87.98	2635.27	

Table 8. Results for the calibrated case on the ETH3D dataset [56]. Opt.: S, R, R_s - PoseLib [37] implementation using Sampson error (S), reprojection error (R) or reprojection error with shift considered (R_s), H - hybrid RANSAC from [67], M - non-linear optimization used in [39].

Depth	Solver	Opt.	SP+LG [14, 42]			RoMA [18]		
			$\epsilon(^{\circ}) \downarrow$	mAA \uparrow	$\tau(ms) \downarrow$	$\epsilon(^{\circ}) \downarrow$	mAA \uparrow	$\tau(ms) \downarrow$
-	5PT [49]	S	1.42	76.56	63.79	0.78	86.18	264.61
Real Depth	Rel3PT [1]	S	1.40	77.23	146.21	0.78	86.24	726.88
	P3P [15]	S	1.39	77.61	34.92	0.78	86.48	158.59
	3PT _{suiv} (M) [67]	S	1.39	77.47	41.69	0.78	86.37	133.69
	3PT _{suiv} (ours)	S	1.39	77.47	29.45	0.78	86.38	118.89
	P3P [15]	R	0.46	90.65	14.73	0.29	94.32	59.42
	3PT _{suiv} (M) [67]	R	<u>0.46</u>	<u>90.68</u>	24.98	<u>0.29</u>	<u>94.32</u>	50.49
	3PT _{suiv} (ours)	R	0.46	90.70	13.04	0.29	94.32	37.90
	P3P [15]	R _s	0.75	87.28	16.01	0.48	92.27	64.69
	3PT _{suiv} (M) [67]	R _s	0.77	86.78	25.58	0.49	91.91	51.34
	3PT _{suiv} (ours)	R _s	0.77	86.78	14.63	0.49	91.92	<u>39.78</u>
	3PT _{suiv} (M) [67]	H [67]	0.98	84.04	714.12	0.62	89.51	1701.35
	3PT _{suiv} (ours)	H [67]	0.98	84.03	705.92	0.62	89.52	1681.53
MiDas [8]	Rel3PT [1]	S	9.22	55.52	44.63	1.65	70.53	177.33
	P3P [15]	S	1.58	72.18	27.33	0.83	84.09	111.49
	3PT _{suiv} (M) [67]	S	1.43	76.66	34.35	0.78	86.10	88.11
	3PT _{suiv} (ours)	S	<u>1.44</u>	<u>76.48</u>	22.98	<u>0.78</u>	<u>85.82</u>	73.67
	P3P [15]	R	24.24	4.97	15.65	22.29	6.37	70.82
	3PT _{suiv} (M) [67]	R	24.22	4.98	24.05	22.44	6.38	49.42
	3PT _{suiv} (ours)	R	24.36	4.96	12.99	22.53	6.28	37.34
	P3P [15]	R _s	18.71	13.20	16.09	16.79	16.19	64.14
	3PT _{suiv} (M) [67]	R _s	14.55	18.78	25.52	11.75	24.35	48.92
	3PT _{suiv} (ours)	R _s	14.71	18.65	<u>15.31</u>	11.83	24.23	<u>37.41</u>
	3PT _{suiv} (M) [67]	H [67]	2.03	69.17	934.38	1.08	81.45	2078.11
	3PT _{suiv} (ours)	H [67]	2.03	69.17	922.74	1.08	81.44	2051.80
DA v2 [66]	Rel3PT [1]	S	5.35	53.60	44.38	1.52	66.28	177.96
	P3P [15]	S	1.44	75.57	29.79	0.78	86.09	127.26
	3PT _{suiv} (M) [67]	S	1.41	76.93	35.16	0.78	86.23	95.37
	3PT _{suiv} (ours)	S	<u>1.41</u>	<u>76.92</u>	23.80	<u>0.78</u>	<u>86.21</u>	81.93
	P3P [15]	R	14.28	23.17	16.09	12.67	26.26	72.41
	3PT _{suiv} (M) [67]	R	14.27	23.12	24.17	12.59	26.30	49.82
	3PT _{suiv} (ours)	R	14.26	23.13	12.99	12.60	26.29	38.09
	P3P [15]	R _s	10.79	31.81	16.71	8.85	36.99	69.50
	3PT _{suiv} (M) [67]	R _s	10.15	33.06	25.21	7.38	40.20	49.51
	3PT _{suiv} (ours)	R _s	10.19	33.03	<u>14.96</u>	7.40	40.13	<u>38.66</u>
	3PT _{suiv} (M) [67]	H [67]	1.91	72.85	878.70	1.14	83.37	1864.97
	3PT _{suiv} (ours)	H [67]	1.90	72.82	867.00	1.14	83.36	1845.20
MoGe [62]	Rel3PT [1]	S	8.12	53.40	55.85	1.69	67.22	221.06
	P3P [15]	S	1.40	77.37	32.95	0.78	86.42	148.76
	3PT _{suiv} (M) [67]	S	1.40	77.24	38.42	0.78	86.38	116.49
	3PT _{suiv} (ours)	S	1.40	77.24	26.66	0.78	86.40	102.31
	P3P [15]	R	2.53	72.05	15.39	2.17	76.15	66.88
	3PT _{suiv} (M) [67]	R	2.52	72.10	24.58	2.18	76.16	50.25
	3PT _{suiv} (ours)	R	2.53	72.08	12.90	2.18	76.14	38.02
	P3P [15]	R _s	2.34	72.52	16.53	1.82	78.46	69.56
	3PT _{suiv} (M) [67]	R _s	2.65	68.71	25.40	1.89	76.93	51.40
	3PT _{suiv} (ours)	R _s	2.66	68.67	<u>14.74</u>	1.89	76.95	<u>40.08</u>
	3PT _{suiv} (M) [67]	H [67]	<u>1.27</u>	<u>80.28</u>	788.18	0.87	<u>86.85</u>	1753.49
	3PT _{suiv} (ours)	H [67]	1.27	80.28	780.57	0.87	86.85	1737.27
UniDepth [51]	Rel3PT [1]	S	4.07	51.60	52.49	1.33	67.56	214.73
	P3P [15]	S	1.40	77.47	34.30	0.78	86.43	150.95
	3PT _{suiv} (M) [67]	S	1.40	77.33	40.31	0.78	86.37	119.66
	3PT _{suiv} (ours)	S	1.40	77.33	28.19	<u>0.78</u>	86.38	105.03
	P3P [15]	R	1.73	79.31	15.44	1.61	81.24	67.38
	3PT _{suiv} (M) [67]	R	1.73	79.30	25.03	1.61	81.19	51.46
	3PT _{suiv} (ours)	R	1.73	79.30	13.21	1.62	81.18	39.11
	P3P [15]	R _s	1.63	78.65	16.46	1.42	82.22	69.20
	3PT _{suiv} (M) [67]	R _s	1.69	77.72	25.56	1.49	81.06	51.66
	3PT _{suiv} (ours)	R _s	1.69	77.71	<u>14.72</u>	1.49	81.07	<u>40.20</u>
	3PT _{suiv} (M) [67]	H [67]	1.15	82.09	720.34	0.78	87.60	1695.57
	3PT _{suiv} (ours)	H [67]	<u>1.15</u>	<u>82.08</u>	713.58	0.78	<u>87.60</u>	1678.83

Depth	Solver	Opt.	Mast3r [39]		
			$\epsilon(^{\circ}) \downarrow$	mAA \uparrow	$\tau(ms) \downarrow$
-	5PT [49]	S	1.14	81.66	137.75
Mast3r [39]	Rel3PT [1]	S	1.13	80.83	149.86
	P3P [15]	S	1.13	81.50	66.06
	3PT _{suiv} (M) [67]	S	<u>1.12</u>	<u>81.40</u>	45.03
	3PT _{suiv} (ours)	S	1.12	81.39	33.73
	P3P [15]	R	22.69	15.88	36.56
	3PT _{suiv} (M) [67]	R	22.81	15.86	30.03
	3PT _{suiv} (ours)	R	22.83	15.83	<u>19.87</u>
	P3P [15]	R _s	21.28	18.01	36.74
	3PT _{suiv} (M) [67]	R _s	28.49	14.10	27.77
	3PT _{suiv} (ours)	R _s	28.63	14.11	18.63
	3PT _{suiv} (M) [67]	H [67]	2.10	72.14	2154.89
	3PT _{suiv} (ours)	H [67]	2.10	72.16	2136.39

Table 9. Results for the calibrated case on the Phototourism dataset [30]. Opt.: S, R, R_s - PoseLib [37] implementation using Sampson error (S), reprojection error (R) or reprojection error with shift considered (R_s), H - hybrid RANSAC from [67], M - non-linear optimization used in [39].

Depth	Solver	Opt.	SP+LG [14, 42]			RoMA [18]		
			$\epsilon(^{\circ}) \downarrow$	mAA \uparrow	$\tau(ms) \downarrow$	$\epsilon(^{\circ}) \downarrow$	mAA \uparrow	$\tau(ms) \downarrow$
-	5PT [49]	S	6.98	37.95	50.27	3.64	56.18	209.19
Real Depth	Rel3PT [1]	S	6.90	38.28	74.72	3.61	56.63	381.28
	P3P [15]	S	6.60	39.58	24.48	3.60	56.67	107.58
	3PT _{suiv} (M) [67]	S	6.70	39.09	34.27	3.62	56.58	92.19
	3PT _{suiv} (ours)	S	6.72	38.98	21.39	3.61	56.65	85.04
	P3P [15]	R	5.54	43.78	<u>13.27</u>	3.42	59.36	52.49
	3PT _{suiv} (M) [67]	R	5.51	43.89	24.24	3.43	<u>59.37</u>	41.09
	3PT _{suiv} (ours)	R	<u>5.52</u>	<u>43.85</u>	11.99	3.43	59.39	33.88
	P3P [15]	R _s	6.07	40.90	14.42	3.51	58.95	55.93
	3PT _{suiv} (M) [67]	R _s	7.33	36.49	26.67	3.58	56.63	42.97
	3PT _{suiv} (ours)	R _s	7.29	36.53	14.84	3.59	56.50	<u>34.86</u>
	3PT _{suiv} (M) [67]	H [67]	5.82	41.90	1756.20	<u>3.42</u>	59.05	4206.15
	3PT _{suiv} (ours)	H [67]	5.80	41.97	1737.82	3.43	59.05	4064.46
MiDas [8]	Rel3PT [1]	S	8.34	34.07	43.34	3.93	53.43	207.44
	P3P [15]	S	<u>6.85</u>	38.39	24.73	3.70	55.91	103.26
	3PT _{suiv} (M) [67]	S	6.84	38.53	32.39	3.64	56.44	78.69
	3PT _{suiv} (ours)	S	6.86	<u>38.48</u>	19.90	<u>3.64</u>	<u>56.41</u>	74.16
	P3P [15]	R	17.89	12.30	<u>13.89</u>	13.34	17.42	58.59
	3PT _{suiv} (M) [67]	R	17.83	12.34	23.98	13.33	17.47	41.70
	3PT _{suiv} (ours)	R	17.81	12.36	11.96	13.31	17.55	<u>34.56</u>
	P3P [15]	R _s	14.19	17.94	14.67	10.20	24.59	56.72
	3PT _{suiv} (M) [67]	R _s	13.24	19.86	26.03	8.78	29.77	40.27
	3PT _{suiv} (ours)	R _s	13.26	19.51	14.37	8.80	29.73	32.78
	3PT _{suiv} (M) [67]	H [67]	7.03	37.56	998.68	3.84	54.97	1780.84
	3PT _{suiv} (ours)	H [67]	7.03	37.49	983.36	3.84	54.93	1755.98
DA v2 [66]	Rel3PT [1]	S	8.33	33.95	42.50	3.96	53.30	203.95
	P3P [15]	S	6.99	37.79	23.98	3.70	55.68	98.12
	3PT _{suiv} (M) [67]	S	6.89	38.50	34.61	3.63	56.43	91.84
	3PT _{suiv} (ours)	S	<u>6.91</u>	<u>38.52</u>	21.90	<u>3.63</u>	<u>56.43</u>	86.06
	P3P [15]	R	23.12	5.87	<u>13.26</u>	19.47	7.45	56.69
	3PT _{suiv} (M) [67]	R	23.35	5.70	25.05	19.35	7.40	45.12
	3PT _{suiv} (ours)	R	23.36	5.66	12.27	19.35	7.39	37.25
	P3P [15]	R _s	16.59	12.99	14.08	12.23	18.64	53.23
	3PT _{suiv} (M) [67]	R _s	13.02	18.83	27.50	8.27	30.91	45.52
	3PT _{suiv} (ours)	R _s	13.02	18.69	15.28	8.22	31.06	<u>37.90</u>
	3PT _{suiv} (M) [67]	H [67]	7.21	36.70	931.97	3.92	54.51	1764.65
	3PT _{suiv} (ours)	H [67]	7.20	36.68	916.70	3.93	54.52	1744.47
MoGe [62]	Rel3PT [1]	S	8.68	33.50	48.65	4.01	52.56	229.08
	P3P [15]	S	6.71	39.23	26.36	3.60	56.57	116.72
	3PT _{suiv} (M) [67]	S	6.71	39.28	35.99	3.62	56.53	97.38
	3PT _{suiv} (ours)	S	6.72	39.19	22.58	3.63	56.49	93.10
	P3P [15]	R	6.37	39.41	<u>14.25</u>	4.32	53.40	58.35
	3PT _{suiv} (M) [67]	R	6.31	39.60	25.45	4.32	53.45	45.60
	3PT _{suiv} (ours)	R	6.31	39.63	12.53	4.32	53.45	<u>37.86</u>
	P3P [15]	R _s	6.73	37.99	15.09	4.07	54.91	59.33
	3PT _{suiv} (M) [67]	R _s	6.80	37.07</				

Depth	Solver	Opt.	SP+LG [14, 42]					RoMA [18]				
			$\epsilon(^{\circ}) \downarrow$	$\epsilon_f \downarrow$	mAA \uparrow	mAA \uparrow	$\tau(ms) \downarrow$	$\epsilon(^{\circ}) \downarrow$	$\epsilon_f \downarrow$	mAA \uparrow	mAA \uparrow	$\tau(ms) \downarrow$
-	6PT [38]	S	2.05	0.04	75.57	61.52	80.02	1.15	0.02	85.23	75.03	147.48
-	3pd [17]	S	2.46	0.04	78.00	62.83	30.70	0.93	0.02	85.98	74.98	113.30
-	4PT _{non} /f(M) [67]	S	1.83	0.03	78.86	63.71	112.34	0.99	0.02	86.37	75.21	167.49
-	4PT _{non} /f(ours)	S	1.72	0.03	78.90	63.56	51.10	1.03	0.02	86.25	75.34	107.05
-	3PT _{non} /f(ours)	S	1.75	0.03	79.17	63.63	25.11	0.99	0.02	86.68	74.99	79.96
-	3PT _{non} /f(ours)	S	1.77	0.04	77.56	62.33	18.72	0.99	0.02	86.42	74.77	72.35
-	4PT _{non} /f(M) [67]	R	0.41	0.01	91.57	87.77	105.13	0.29	0.00	93.06	90.15	149.04
-	4PT _{non} /f(ours)	R	0.41	0.01	91.88	87.92	44.28	0.29	0.00	93.14	90.04	88.67
-	3PT _{non} /f(ours)	R	0.21	0.01	91.32	87.66	19.48	0.29	0.00	92.33	90.04	66.85
-	3PT _{non} /f(ours)	R	0.40	0.01	91.61	88.65	10.49	0.22	0.00	93.59	90.48	61.25
-	4PT _{non} /f(M) [67]	R _s	0.50	0.01	90.26	84.96	106.97	0.34	0.01	92.30	88.51	154.70
-	4PT _{non} /f(ours)	R _s	0.50	0.01	90.33	84.99	46.15	0.34	0.01	92.33	88.63	94.59
-	3PT _{non} /f(ours)	R _s	0.49	0.01	90.52	85.04	20.05	0.30	0.00	92.81	88.95	67.22
-	3PT _{non} /f(ours)	R _s	0.48	0.01	90.67	85.66	14.00	0.33	0.00	93.00	89.00	61.62
-	4PT _{non} /f(M) [67]	H [67]	1.07	0.02	82.01	75.63	1502.02	2.12	0.02	76.69	72.51	3218.22
-	4PT _{non} /f(ours)	H [67]	1.07	0.02	82.19	75.76	1411.05	2.28	0.02	76.42	72.43	3067.57
-	3pd [17]	S	4.08	0.07	61.91	49.69	25.35	1.91	0.02	78.71	68.10	86.60
-	4PT _{non} /f(M) [67]	S	2.17	0.04	73.99	59.89	103.86	1.14	0.02	85.11	74.93	142.78
-	4PT _{non} /f(ours)	S	2.26	0.04	73.53	59.35	45.74	1.10	0.02	84.86	74.80	84.62
-	3PT _{non} /f(ours)	S	2.26	0.04	73.11	60.88	21.36	1.25	0.02	84.66	74.47	65.79
-	3PT _{non} /f(ours)	S	9.25	0.16	52.77	41.40	12.76	5.32	0.05	70.75	60.27	48.01
-	4PT _{non} /f(M) [67]	R	14.47	0.19	24.45	25.80	11.06	0.19	30.87	26.96	129.24	
-	4PT _{non} /f(ours)	R	14.56	0.20	24.04	25.42	41.15	11.16	0.19	30.65	27.07	71.31
-	3PT _{non} /f(ours)	R	18.29	0.24	22.02	22.85	9.15	12.95	0.21	29.01	25.81	26.22
-	4PT _{non} /f(M) [67]	R _s	8.46	0.14	36.05	34.35	101.66	6.29	0.11	46.33	38.06	138.43
-	4PT _{non} /f(ours)	R _s	8.60	0.14	36.05	34.09	43.58	6.36	0.11	46.47	38.10	80.46
-	3PT _{non} /f(ours)	R _s	8.56	0.14	35.48	34.10	19.15	6.47	0.12	45.22	38.08	62.22
-	3PT _{non} /f(ours)	R _s	13.22	0.19	31.71	29.83	9.48	9.26	0.15	41.05	33.72	36.18
-	4PT _{non} /f(M) [67]	H [67]	2.58	0.05	68.70	56.01	1303.38	1.48	0.03	81.10	67.25	2301.37
-	4PT _{non} /f(ours)	H [67]	2.47	0.05	69.87	56.45	1316.09	1.48	0.03	81.44	67.03	2140.90
-	3pd [17]	S	4.54	0.08	61.60	48.76	27.01	2.07	0.02	78.86	68.29	91.39
-	4PT _{non} /f(M) [67]	S	2.10	0.04	74.60	60.77	104.75	1.21	0.02	85.33	75.09	146.35
-	4PT _{non} /f(ours)	S	2.02	0.04	74.67	60.41	46.62	1.20	0.02	85.61	75.43	88.03
-	3PT _{non} /f(ours)	S	2.20	0.04	73.66	60.93	21.62	1.23	0.02	84.89	75.00	67.61
-	3PT _{non} /f(ours)	S	12.16	0.20	49.70	39.23	12.56	6.20	0.06	67.86	57.93	46.57
-	4PT _{non} /f(M) [67]	R	13.22	0.18	26.18	28.41	100.09	10.98	0.18	32.52	30.93	134.01
-	4PT _{non} /f(ours)	R	13.16	0.18	26.12	28.05	42.01	10.95	0.17	32.71	31.17	75.68
-	3PT _{non} /f(ours)	R	13.44	0.19	26.23	28.12	18.64	11.16	0.17	32.68	31.01	63.33
-	3PT _{non} /f(ours)	R	17.08	0.26	24.19	25.57	8.92	11.90	0.21	31.29	28.65	35.25
-	4PT _{non} /f(M) [67]	R _s	6.31	0.10	44.42	39.84	102.76	4.75	0.08	53.63	44.53	145.36
-	4PT _{non} /f(ours)	R _s	6.32	0.10	43.88	38.12	44.51	4.72	0.08	53.87	45.28	87.17
-	3PT _{non} /f(ours)	R _s	7.45	0.12	41.38	38.13	19.63	5.55	0.09	50.94	44.24	65.92
-	3PT _{non} /f(ours)	R _s	13.04	0.21	35.07	30.57	9.36	8.41	0.13	45.70	38.04	35.85
-	4PT _{non} /f(M) [67]	H [67]	2.34	0.05	70.07	58.00	1190.89	1.28	0.03	81.56	68.72	2161.36
-	4PT _{non} /f(ours)	H [67]	2.33	0.05	70.16	58.31	1216.89	1.30	0.03	81.57	68.68	2245.95
-	3pd [17]	S	3.18	0.06	68.24	54.64	27.70	1.56	0.02	80.98	70.19	98.44
-	4PT _{non} /f(M) [67]	S	2.15	0.04	76.06	61.81	107.39	1.02	0.02	85.61	75.61	151.65
-	4PT _{non} /f(ours)	S	2.15	0.04	75.59	60.88	57.91	1.10	0.02	85.85	75.80	92.92
-	3PT _{non} /f(ours)	S	1.99	0.04	76.94	62.66	24.72	1.05	0.02	86.04	75.83	75.12
-	3PT _{non} /f(ours)	S	9.42	0.16	52.38	41.58	14.47	5.54	0.06	70.95	61.14	54.72
-	4PT _{non} /f(M) [67]	R	2.59	0.04	69.92	62.11	102.45	1.91	0.03	76.56	65.93	138.82
-	4PT _{non} /f(ours)	R	2.68	0.04	69.37	62.00	52.91	1.96	0.03	76.55	65.80	79.71
-	3PT _{non} /f(ours)	R	2.56	0.04	70.86	63.26	21.40	1.95	0.04	77.77	66.04	92.94
-	3PT _{non} /f(ours)	R	5.74	0.06	61.30	54.62	10.30	3.15	0.04	71.39	61.14	41.74
-	4PT _{non} /f(M) [67]	R _s	2.53	0.05	69.12	57.39	104.99	1.92	0.04	77.16	63.83	148.77
-	4PT _{non} /f(ours)	R _s	2.63	0.05	68.87	57.18	55.04	1.87	0.04	77.10	63.82	89.96
-	3PT _{non} /f(ours)	R _s	2.49	0.05	70.04	58.86	22.20	1.95	0.04	77.46	64.31	74.67
-	3PT _{non} /f(ours)	R _s	6.30	0.07	60.26	50.42	10.64	3.16	0.04	71.44	58.33	41.99
-	4PT _{non} /f(M) [67]	H [67]	1.50	0.03	79.23	66.34	956.33	0.89	0.02	86.99	76.66	1923.31
-	4PT _{non} /f(ours)	H [67]	1.41	0.03	80.24	67.42	967.52	0.91	0.02	87.20	76.50	2043.91
-	3pd [17]	S	3.49	0.07	69.47	55.57	27.57	1.89	0.02	82.50	71.89	97.99
-	4PT _{non} /f(M) [67]	S	2.21	0.04	75.61	61.37	106.73	1.12	0.02	85.63	75.66	151.31
-	4PT _{non} /f(ours)	S	1.92	0.04	76.18	62.00	46.97	1.12	0.02	85.59	75.64	91.92
-	3PT _{non} /f(ours)	S	2.04	0.04	76.89	62.42	23.47	1.04	0.02	85.78	75.69	75.62
-	3PT _{non} /f(ours)	S	3.98	0.07	63.26	51.81	15.52	2.20	0.02	79.68	69.89	59.07
-	4PT _{non} /f(M) [67]	R	2.70	0.04	69.55	59.49	101.94	2.07	0.04	76.35	63.30	139.31
-	4PT _{non} /f(ours)	R	2.69	0.04	69.50	59.62	42.12	2.11	0.04	76.21	63.44	79.50
-	3PT _{non} /f(ours)	R	2.68	0.05	69.61	59.84	20.48	2.07	0.04	76.25	63.64	75.00
-	3PT _{non} /f(ours)	R	2.78	0.05	68.11	58.68	11.64	2.10	0.04	75.89	63.05	48.44
-	4PT _{non} /f(M) [67]	R _s	2.67	0.05	69.03	58.06	104.79	1.89	0.03	77.33	64.83	149.96
-	4PT _{non} /f(ours)	R _s	2.65	0.05	68.79	58.11	44.72	1.88	0.03	77.14	64.62	90.69
-	3PT _{non} /f(ours)	R _s	2.51	0.05	69.22	59.00	21.45	1.94	0.03	77.02	64.61	77.26
-	3PT _{non} /f(ours)	R _s	2.74	0.05	67.70	57.35	12.22	1.90	0.03	76.91	64.55	49.48
-	4PT _{non} /f(M) [67]	H [67]	1.27	0.03	81.68	69.64	1107.04	0.83	0.02	87.30	77.34	1997.88
-	4PT _{non} /f(ours)	H [67]	1.26	0.03	81.99	69.28	1149.25	0.82	0.02	87.53	77.79	2133.46

Table 11. Results for the case of two cameras with shared unknown focal length on the ETH3D dataset [56]. Opt.: S, R, R_s - PoseLib [37] implementation using Sampson error (S), reprojection error (R) or reprojection error with shift considered (R_s), H - hybrid RANSAC from [67], M - non-linear optimization used in [39].

Depth	Solver	Opt.	SP+LG [14, 42]					RoMA [18]				
			$\epsilon(^{\circ}) \downarrow$	$\epsilon_f \downarrow$	mAA \uparrow	mAA \uparrow	$\tau(ms) \downarrow$	$\epsilon(^{\circ}) \downarrow$	$\epsilon_f \downarrow$	mAA \uparrow	mAA \uparrow	$\tau(ms) \downarrow$
-	6PT [38]	S	10.54	0.14	28.39	25.51	71.04	4.78	0.05	48.67	47.45	139.19
-	3pd [17]	S	10.01	0.14	28.80	26.17	19.87	4.76	0.05	48.91	47.42	82.15
-	4PT _{non} /f(M) [67]	S	9.12	0.13	30.12	27.82	93.60	4.77	0.05	49.16	48.20	114.10
-	4PT											

Depth	Solver	Opt.	SP+LG [14, 42]					RoMA [18]				
			$\epsilon^{\circ} \downarrow$	$\epsilon_f \downarrow$	mAA \uparrow	mAA \uparrow	$\tau(ms) \downarrow$	$\epsilon^{\circ} \downarrow$	$\epsilon_f \downarrow$	mAA \uparrow	mAA \uparrow	$\tau(ms) \downarrow$
-	7PT [27]	S	4.55	0.17	54.17	36.19	18.41	2.46	0.05	71.94	56.85	61.02
Real Depth	4p4d [17]	S	3.80	0.10	57.55	37.99	17.95	2.18	0.05	72.70	56.65	65.62
	4PT _{www} _{f1,2} (M) [67]	S	3.73	0.09	60.21	39.12	19.02	1.96	0.04	75.42	57.35	157.06
	4PT _{www} _{f1,2} (ours)	S	3.55	0.10	60.40	38.75	20.35	2.05	0.04	75.24	57.09	89.33
	3PT _{www} _{f1,2} (ours)	S	3.39	0.09	61.56	39.71	18.18	2.02	0.04	75.96	57.99	73.89
	3PT _{www} _{f1,2} (ours)	S	3.63	0.09	61.46	39.60	21.81	1.92	0.04	75.96	57.67	84.35
	4PT _{www} _{f1,2} (M) [67]	R	0.67	0.01	88.65	86.27	88.59	0.43	0.00	91.34	89.35	122.85
	4PT _{www} _{f1,2} (ours)	R	0.68	0.01	88.60	86.20	20.93	0.42	0.00	91.49	89.50	54.34
	3PT _{www} _{f1,2} (ours)	R	0.64	0.01	89.18	86.84	8.98	0.42	0.00	91.84	89.82	40.03
	4PT _{www} _{f1,2} (M) [67]	R _s	0.92	0.01	86.32	83.40	13.66	0.54	0.01	90.36	87.66	55.86
	4PT _{www} _{f1,2} (ours)	R _s	0.93	0.01	86.06	83.88	90.19	0.58	0.01	89.92	87.29	128.38
	3PT _{www} _{f1,2} (ours)	R _s	0.93	0.01	86.03	83.04	22.50	0.58	0.01	89.95	87.39	58.50
	4PT _{www} _{f1,2} (ours)	R _s	0.88	0.01	86.69	83.73	10.02	0.54	0.01	90.56	87.84	41.63
3PT _{www} _{f1,2} (ours)	R _s	0.92	0.01	86.32	83.40	13.66	0.54	0.01	90.36	87.66	55.86	
4PT _{www} _{f1,2} (M) [67]	H [67]	2.11	0.02	77.88	72.52	1838.11	1.99	0.02	76.18	70.63	4016.40	
3PT _{www} _{f1,2} (ours)	H [67]	2.15	0.02	78.23	72.93	1741.36	1.96	0.02	76.23	70.70	3584.62	
MidDas [8]	4p4d [17]	S	7.13	0.15	46.45	30.84	14.83	2.64	0.05	67.34	52.94	51.51
	4PT _{www} _{f1,2} (M) [67]	S	5.14	0.10	53.00	36.05	88.47	2.42	0.05	71.64	56.16	129.33
	4PT _{www} _{f1,2} (ours)	S	4.87	0.11	52.76	35.88	24.01	2.44	0.04	71.73	56.25	62.74
	3PT _{www} _{f1,2} (ours)	S	5.15	0.12	52.89	34.57	13.60	2.78	0.05	70.19	55.15	54.98
	3PT _{www} _{f1,2} (ours)	S	6.37	0.13	50.18	32.46	17.33	3.46	0.06	68.97	53.08	65.10
	4PT _{www} _{f1,2} (M) [67]	R	18.78	0.21	23.23	23.43	83.69	14.14	0.20	31.98	26.12	105.79
	4PT _{www} _{f1,2} (ours)	R	19.31	0.21	22.73	23.13	18.56	14.44	0.20	31.60	25.65	39.00
	3PT _{www} _{f1,2} (ours)	R	19.65	0.21	23.90	23.74	8.00	14.60	0.20	31.51	25.90	34.57
	4PT _{www} _{f1,2} (M) [67]	R _s	19.76	0.21	24.10	23.94	12.33	14.07	0.21	33.77	29.47	46.89
	4PT _{www} _{f1,2} (ours)	R _s	15.40	0.19	28.40	27.58	8.90	11.02	0.15	38.04	31.91	112.86
	3PT _{www} _{f1,2} (ours)	R _s	17.81	0.19	27.49	26.78	20.11	11.41	0.15	37.79	32.02	45.86
	4PT _{www} _{f1,2} (ours)	R _s	15.05	0.18	28.36	27.62	9.05	11.32	0.16	37.55	31.36	26.96
3PT _{www} _{f1,2} (ours)	R _s	16.50	0.18	27.40	26.57	12.41	11.91	0.17	36.42	30.24	38.33	
4PT _{www} _{f1,2} (M) [67]	H [67]	3.87	0.08	61.54	45.60	2095.25	2.24	0.06	73.42	54.05	3348.48	
3PT _{www} _{f1,2} (ours)	H [67]	3.91	0.08	61.69	46.15	2098.90	2.24	0.06	73.51	54.31	3356.13	
DA v2 [66]	4p4d [17]	S	6.82	0.13	47.06	31.27	15.28	2.74	0.05	69.66	54.57	52.90
	4PT _{www} _{f1,2} (M) [67]	S	4.41	0.10	53.03	36.66	89.93	2.23	0.04	73.11	57.15	132.70
	4PT _{www} _{f1,2} (ours)	S	4.14	0.10	55.65	37.45	24.63	2.29	0.05	72.84	52.12	67.11
	3PT _{www} _{f1,2} (ours)	S	4.76	0.11	53.09	35.21	14.07	2.45	0.04	71.54	56.14	55.95
	3PT _{www} _{f1,2} (ours)	S	6.41	0.14	49.68	33.58	17.75	4.10	0.06	67.76	52.32	67.40
	4PT _{www} _{f1,2} (M) [67]	R	14.80	0.17	29.09	27.35	84.32	11.17	0.16	36.37	30.37	109.49
	4PT _{www} _{f1,2} (ours)	R	14.79	0.17	29.14	27.35	18.93	11.36	0.16	36.19	30.59	42.60
	3PT _{www} _{f1,2} (ours)	R	14.82	0.16	28.92	27.71	8.24	12.04	0.16	36.40	30.58	37.01
	4PT _{www} _{f1,2} (M) [67]	R _s	15.11	0.18	28.82	27.42	12.45	12.46	0.17	35.71	30.24	47.30
	4PT _{www} _{f1,2} (ours)	R _s	9.54	0.12	36.11	34.23	85.43	6.79	0.10	45.45	39.65	118.26
	3PT _{www} _{f1,2} (ours)	R _s	9.62	0.12	36.03	34.10	20.74	6.88	0.10	44.99	39.57	51.19
	4PT _{www} _{f1,2} (ours)	R _s	10.18	0.13	35.65	33.16	9.60	7.54	0.12	43.69	37.85	29.63
3PT _{www} _{f1,2} (ours)	R _s	11.24	0.15	34.35	31.61	12.62	8.12	0.13	42.68	36.90	48.98	
4PT _{www} _{f1,2} (M) [67]	H [67]	3.60	0.08	61.64	45.60	1896.45	2.18	0.06	72.14	54.95	3128.59	
3PT _{www} _{f1,2} (ours)	H [67]	3.50	0.08	61.86	46.25	1894.68	2.23	0.06	73.31	55.02	3097.87	
MoGe [62]	4p4d [17]	S	4.98	0.11	52.91	36.19	16.30	2.40	0.05	71.59	56.53	59.06
	4PT _{www} _{f1,2} (M) [67]	S	4.07	0.09	57.28	38.04	90.86	2.22	0.04	73.47	57.08	138.85
	4PT _{www} _{f1,2} (ours)	S	3.91	0.10	57.16	37.69	26.93	2.21	0.04	73.21	57.23	71.54
	3PT _{www} _{f1,2} (ours)	S	4.76	0.11	53.09	35.21	14.07	2.45	0.04	71.54	56.14	55.95
	3PT _{www} _{f1,2} (ours)	S	6.40	0.14	49.68	33.58	17.75	4.10	0.06	67.76	52.32	67.40
	4PT _{www} _{f1,2} (M) [67]	R	14.80	0.17	29.09	27.35	84.32	11.17	0.16	36.37	30.37	109.49
	4PT _{www} _{f1,2} (ours)	R	14.79	0.17	29.14	27.35	18.93	11.36	0.16	36.19	30.59	42.60
	3PT _{www} _{f1,2} (ours)	R	14.82	0.16	28.92	27.71	8.24	12.04	0.16	36.40	30.58	37.01
	4PT _{www} _{f1,2} (M) [67]	R _s	15.11	0.18	28.82	27.42	12.45	12.46	0.17	35.71	30.24	47.30
	4PT _{www} _{f1,2} (ours)	R _s	9.54	0.12	36.11	34.23	85.43	6.79	0.10	45.45	39.65	118.26
	3PT _{www} _{f1,2} (ours)	R _s	9.62	0.12	36.03	34.10	20.74	6.88	0.10	44.99	39.57	51.19
	4PT _{www} _{f1,2} (ours)	R _s	10.18	0.13	35.65	33.16	9.60	7.54	0.12	43.69	37.85	29.63
3PT _{www} _{f1,2} (ours)	R _s	11.24	0.15	34.35	31.61	12.62	8.12	0.13	42.68	36.90	48.98	
4PT _{www} _{f1,2} (M) [67]	H [67]	3.60	0.08	61.64	45.60	1896.45	2.18	0.06	72.14	54.95	3128.59	
3PT _{www} _{f1,2} (ours)	H [67]	3.50	0.08	61.86	46.25	1894.68	2.23	0.06	73.31	55.02	3097.87	
MoGe [62]	4p4d [17]	S	4.98	0.11	52.91	36.19	16.30	2.40	0.05	71.59	56.53	59.06
	4PT _{www} _{f1,2} (M) [67]	S	4.07	0.09	57.28	38.04	90.86	2.22	0.04	73.47	57.08	138.85
	4PT _{www} _{f1,2} (ours)	S	3.91	0.10	57.16	37.69	26.93	2.21	0.04	73.21	57.23	71.54
	3PT _{www} _{f1,2} (ours)	S	4.76	0.11	53.09	35.21	14.07	2.45	0.04	71.54	56.14	55.95
	3PT _{www} _{f1,2} (ours)	S	6.40	0.14	49.68	33.58	17.75	4.10	0.06	67.76	52.32	67.40
	4PT _{www} _{f1,2} (M) [67]	R	14.80	0.17	29.09	27.35	84.32	11.17	0.16	36.37	30.37	109.49
	4PT _{www} _{f1,2} (ours)	R	14.79	0.17	29.14	27.35	18.93	11.36	0.16	36.19	30.59	42.60
	3PT _{www} _{f1,2} (ours)	R	14.82	0.16	28.92	27.71	8.24	12.04	0.16	36.40	30.58	37.01
	4PT _{www} _{f1,2} (M) [67]	R _s	15.11	0.18	28.82	27.42	12.45	12.46	0.17	35.71	30.24	47.30
	4PT _{www} _{f1,2} (ours)	R _s	9.54	0.12	36.11	34.23	85.43	6.79	0.10	45.45	39.65	118.26
	3PT _{www} _{f1,2} (ours)	R _s	9.62	0.12	36.03	34.10	20.74	6.88	0.10	44.99	39.57	51.19
	4PT _{www} _{f1,2} (ours)	R _s	10.18	0.13	35.65	33.16	9.60	7.54	0.12	43.69	37.85	29.63
3PT _{www} _{f1,2} (ours)	R _s	11.24	0.15	34.35	31.61	12.62	8.12	0.13	42.68	36.90	48.98	
4PT _{www} _{f1,2} (M) [67]	H [67]	3.60	0.08	61.64	45.60	1896.45	2.18	0.06	72.14	54.95	3128.59	
3PT _{www} _{f1,2} (ours)	H [67]	3.50	0.08	61.86	46.25	1894.68	2.23	0.06	73.31	55.02	3097.87	
UniDepth [51]	4p4d [17]	S	5.26	0.11	52.71	35.74	16.46	2.51	0.05	71.03	56.20	58.78
	4PT _{www} _{f1,2} (M) [67]	S	3.78	0.10	57.41	37.66	91.97	2.30	0.05	73.06	57.01	138.56
	4PT _{www} _{f1,2} (ours)	S	4.22	0.10	57.07	37.57	25.63	2.34	0.04	73.14	57.16	70.39
	3PT _{www} _{f1,2}											

Depth	Solver	Opt.	SP4LG [14, 42]				RoMA [18]					
			$\epsilon(^{\circ}) \downarrow$	$e_f \downarrow$	mAA \uparrow	mAA \uparrow	$\tau(ms) \downarrow$	$\epsilon(^{\circ}) \downarrow$	$e_f \downarrow$	mAA \uparrow	mAA \uparrow	$\tau(ms) \downarrow$
Real Depth	7PT [27]	S	17.38	0.19	17.90	18.87	16.87	6.75	0.08	37.74	35.25	60.31
	4p4d [17]	S	15.37	0.19	18.01	17.69	14.09	6.61	0.08	38.11	35.43	55.64
	4PT _{non-f_{1,2}(M)} [67]	S	15.84	0.20	18.42	19.19	88.28	6.54	0.08	38.67	35.87	115.22
	4PT _{non-f_{1,2}(ours)}	S	15.97	0.21	17.80	18.37	25.67	6.49	0.08	38.67	35.96	74.31
	3PT _{non-f_{1,2}(ours)}	S	14.97	0.19	18.79	19.08	16.32	6.44	0.08	39.03	36.21	64.50
	3PT _{non-f_{1,2}(ours)}	S	14.23	0.18	19.22	19.70	18.99	6.46	0.08	38.83	36.05	73.44
	4PT _{non-f_{1,2}(M)} [67]	R	11.89	0.08	25.82	24.78	80.53	5.12	0.04	45.93	55.91	85.85
	4PT _{non-f_{1,2}(ours)}	R	11.97	0.09	25.82	24.59	19.98	5.11	0.04	45.95	55.98	38.51
	3PT _{non-f_{1,2}(ours)}	R	11.76	0.08	26.07	35.06	9.77	5.02	0.04	46.45	56.41	34.33
	3PT _{non-f_{1,2}(ours)}	R	11.71	0.08	26.16	34.74	13.36	5.04	0.04	46.43	56.57	48.19
	4PT _{non-f_{1,2}(ours)}	R _s	17.00	0.16	19.78	23.15	82.22	5.83	0.06	41.17	43.85	96.03
	4PT _{non-f_{1,2}(ours)}	R _s	16.93	0.16	19.85	22.90	22.86	5.88	0.06	40.95	43.59	48.61
	3PT _{non-f_{1,2}(ours)}	R _s	13.07	0.12	23.11	27.49	11.30	5.51	0.05	43.24	47.74	38.84
	3PT _{non-f_{1,2}(ours)}	R _s	12.86	0.12	23.12	27.43	14.36	5.57	0.05	42.97	47.58	52.55
	4PT _{non-f_{1,2}(M)} [67]	H [67]	10.94	0.10	27.01	30.33	3187.44	4.64	0.04	48.82	53.28	6680.16
	3PT _{non-f_{1,2}(ours)}	H [67]	12.20	0.11	24.98	28.98	3006.32	4.96	0.04	47.13	51.78	6266.57
MidDAS [8]	4p4d [17]	S	18.98	0.20	17.13	18.58	14.44	6.90	0.09	37.07	34.38	57.05
	4PT _{non-f_{1,2}(M)} [67]	S	17.76	0.24	16.48	17.60	85.78	6.89	0.08	37.45	35.47	109.98
	4PT _{non-f_{1,2}(ours)}	S	17.54	0.25	16.39	17.54	24.68	6.84	0.09	37.37	34.52	67.68
	3PT _{non-f_{1,2}(ours)}	S	17.00	0.21	17.34	18.50	14.93	6.65	0.08	38.20	35.21	56.94
	3PT _{non-f_{1,2}(ours)}	S	16.12	0.19	17.88	18.80	17.28	6.62	0.08	37.99	35.30	64.37
	4PT _{non-f_{1,2}(M)} [67]	R	26.43	0.19	9.97	16.85	79.24	16.20	0.13	15.42	24.33	83.72
	4PT _{non-f_{1,2}(ours)}	R	26.35	0.19	10.04	16.72	19.69	15.87	0.13	15.82	23.51	36.21
	3PT _{non-f_{1,2}(ours)}	R	25.74	0.19	10.05	16.74	9.85	15.83	0.13	15.79	23.94	34.03
	3PT _{non-f_{1,2}(ours)}	R	25.67	0.19	10.09	17.19	12.96	15.98	0.13	15.82	23.77	44.85
	4PT _{non-f_{1,2}(M)} [67]	R _s	25.95	0.24	10.03	13.87	81.39	15.45	0.15	15.51	21.74	92.21
	4PT _{non-f_{1,2}(ours)}	R _s	25.64	0.24	9.46	14.31	21.88	15.23	0.15	15.79	21.87	43.73
	3PT _{non-f_{1,2}(ours)}	R _s	24.92	0.22	10.01	15.05	10.99	14.78	0.14	15.95	23.01	37.36
	3PT _{non-f_{1,2}(ours)}	R _s	24.75	0.21	9.89	15.46	13.48	14.47	0.14	16.09	22.71	48.16
	4PT _{non-f_{1,2}(M)} [67]	H [67]	13.80	0.13	19.91	23.38	2238.95	6.45	0.08	38.55	36.73	3600.11
	3PT _{non-f_{1,2}(ours)}	H [67]	13.66	0.14	20.03	23.26	2206.62	6.50	0.08	38.31	36.74	3648.22
	DA v2 [66]	4p4d [17]	S	19.91	0.22	16.53	17.73	14.79	6.88	0.09	37.06	35.05
4PT _{non-f_{1,2}(M)} [67]		S	16.20	0.21	17.90	18.49	87.23	6.65	0.08	38.19	36.24	116.51
4PT _{non-f_{1,2}(ours)}		S	16.62	0.22	17.17	18.08	25.66	6.84	0.09	37.83	35.46	73.90
3PT _{non-f_{1,2}(ours)}		S	16.69	0.21	18.21	18.73	15.39	6.60	0.08	38.19	35.50	58.31
3PT _{non-f_{1,2}(ours)}		S	16.85	0.20	17.42	18.87	16.93	6.80	0.08	37.76	35.77	63.67
4PT _{non-f_{1,2}(M)} [67]		R	21.58	0.20	10.70	15.24	80.39	14.57	0.17	15.53	18.47	88.48
4PT _{non-f_{1,2}(ours)}		R	21.91	0.20	10.79	14.88	20.48	14.32	0.17	15.52	18.45	40.65
3PT _{non-f_{1,2}(ours)}		R	21.78	0.20	10.81	15.39	9.92	14.23	0.17	15.47	18.72	34.91
3PT _{non-f_{1,2}(ours)}		R	21.73	0.20	10.87	15.02	11.76	14.41	0.17	15.23	18.42	41.82
4PT _{non-f_{1,2}(M)} [67]		R _s	20.47	0.20	11.58	14.89	82.53	12.07	0.14	19.41	20.37	97.58
4PT _{non-f_{1,2}(ours)}		R _s	20.56	0.21	11.68	15.05	22.72	12.12	0.15	19.28	20.04	50.27
3PT _{non-f_{1,2}(ours)}		R _s	20.19	0.19	11.93	16.09	11.18	12.54	0.14	18.88	20.67	38.21
3PT _{non-f_{1,2}(ours)}		R _s	20.02	0.19	11.92	15.88	12.77	12.38	0.14	18.75	20.65	45.27
4PT _{non-f_{1,2}(M)} [67]		H [67]	14.26	0.14	18.67	20.82	2075.73	6.89	0.09	36.13	32.05	3673.36
3PT _{non-f_{1,2}(ours)}		H [67]	14.34	0.15	18.68	20.63	2044.96	6.99	0.09	35.60	31.74	3665.44
MoGe [62]		4p4d [17]	S	16.82	0.20	18.12	18.76	16.94	6.54	0.08	38.23	35.95
	4PT _{non-f_{1,2}(M)} [67]	S	15.20	0.21	18.90	18.39	87.92	6.48	0.08	38.62	36.23	121.68
	4PT _{non-f_{1,2}(ours)}	S	15.50	0.20	18.33	18.63	26.63	6.45	0.08	38.63	36.26	78.42
	3PT _{non-f_{1,2}(ours)}	S	15.05	0.21	18.58	18.67	17.27	6.44	0.08	38.99	35.98	69.50
	3PT _{non-f_{1,2}(ours)}	S	15.65	0.19	17.80	19.15	19.76	6.47	0.08	38.71	35.76	77.13
	4PT _{non-f_{1,2}(M)} [67]	R	13.72	0.10	22.34	31.46	81.79	6.16	0.05	39.75	50.07	91.97
	4PT _{non-f_{1,2}(ours)}	R	13.84	0.10	22.16	31.33	20.89	6.15	0.05	39.68	49.92	43.28
	3PT _{non-f_{1,2}(ours)}	R	13.50	0.10	22.57	31.56	10.81	6.13	0.05	40.11	50.24	40.11
	3PT _{non-f_{1,2}(ours)}	R	13.82	0.10	22.39	31.81	14.04	6.12	0.05	40.13	49.87	53.29
	4PT _{non-f_{1,2}(M)} [67]	R _s	15.27	0.13	20.54	25.11	84.46	6.58	0.06	37.47	43.04	102.27
	4PT _{non-f_{1,2}(ours)}	R _s	14.97	0.13	20.86	25.34	23.30	6.55	0.06	37.59	43.01	53.65
	3PT _{non-f_{1,2}(ours)}	R _s	14.62	0.13	20.91	25.67	12.65	6.49	0.06	37.79	43.63	45.60
	3PT _{non-f_{1,2}(ours)}	R _s	15.27	0.13	20.82	25.85	15.40	6.44	0.06	37.83	43.36	58.28
	4PT _{non-f_{1,2}(M)} [67]	H [67]	10.49	0.10	26.54	31.47	1794.05	4.82	0.05	47.53	51.04	2925.24
	3PT _{non-f_{1,2}(ours)}	H [67]	10.51	0.09	26.82	31.59	1749.53	4.74	0.05	48.12	51.67	2858.68
	UniDepth [51]	4p4d [17]	S	16.66	0.19	17.86	19.06	17.09	6.52	0.08	38.43	36.12
4PT _{non-f_{1,2}(M)} [67]		S	15.20	0.21	18.35	18.90	88.32	6.39	0.08	39.17	36.25	121.55
4PT _{non-f_{1,2}(ours)}		S	15.48	0.21	18.30	18.54	26.45	6.53	0.08	38.52	36.27	78.39
3PT _{non-f_{1,2}(ours)}		S	14.79	0.19	18.79	18.98	17.47	6.47	0.08	39.05	36.41	68.83
3PT _{non-f_{1,2}(ours)}		S	14.66	0.19	18.72	19.42	19.94	6.29	0.08	39.47	36.61	77.66
4PT _{non-f_{1,2}(M)} [67]		R	13.12	0.10	23.32	31.32	80.63	6.13	0.05	40.14	50.29	91.51
4PT _{non-f_{1,2}(ours)}		R	13.15	0.10	23.38	31.48	20.94	6.11	0.05	40.29	50.30	43.34
3PT _{non-f_{1,2}(ours)}		R	12.78	0.09	23.57	31.94	11.01	6.09	0.05	40.40	50.47	40.35
3PT _{non-f_{1,2}(ours)}		R	12.47	0.09	23.66	32.02	14.00	6.08	0.05	40.45	50.49	53.93
4PT _{non-f_{1,2}(M)} [67]		R _s	14.13	0.13	21.19	24.75	85.47	6.28	0.06	38.89	43.01	102.34
4PT _{non-f_{1,2}(ours)}		R _s	14.16	0.13	20.99	24.92	23.13	6.31	0.06	38.81	43.08	53.91
3PT _{non-f_{1,2}(ours)}		R _s	13.89	0.13	21.29	24.19	12.66	6.28	0.06	38.83	43.37	46.52
3PT _{non-f_{1,2}(ours)}		R _s	13.84	0.13	21.45	24.99	15.44	6.23	0.06	39.13	43.56	59.57
4PT _{non-f_{1,2}(M)} [67]		H [67]	10.76	0.10	27.20	31.21	1765.25	4.77	0.04	47.81	52.12	2906.99
3PT _{non-f_{1,2}(ours)}		H [67]	10.29	0.09	27.82	31.78	1710.72	4.71	0.04	48.26	52.41	2847.16

Depth	Solver	Opt.	Mast3r [39]				
			$\epsilon(^{\circ}) \downarrow$	$e_f \downarrow$	mAA \uparrow	$\tau(ms) \downarrow$	
-	7PT [27]	S	4.01	0.04	54.25	52.79	37.99
Mast3r [39]	4p4d [17]	S	4.07	0.05	53.41	50.67	33.18
	4PT _{non-f_{1,2}(M)} [67]	S	4.39	0.05	50.91	49.03	105.79
	4PT _{non-f_{1,2}(ours)}	S	4.47	0.			